Stabilizing slug control using sub-sea choke valve

Mats Lieungh

June 7, 2012

Abstract

This thesis study the possibility of riser slugging control in offshore oil production using a subsea choke valve. A 5-state simplified model of a well-pipeline-riser system is introduced and fitted to a reference model in the flow simulator OLGA. The models have two inputs, a subsea valve at the wellhead and a topside valve at the top of the riser. The effect the valves have on the behavior of the simplified model are fitted to simulation data from the OLGA-model using bifurcation diagrams.

An input-output controllability analysis of the simplified model show that anti-slug control using a subsea valve at the wellhead is more difficult than the conventional solution, which is to use the topside choke valve. This is confirmed by simulations on the simplified model using $\mathcal{H}_\infty$-controllers.

Stabilizing control of the OLGA-model using the subsea valve was unsuccessful, despite testing different measurement combinations and control structures. A more promising solution for controlling riser slugging using a subsea valve is tested in OLGA, where a subsea valve located near the base of the riser can keep the system stable at riser slugging conditions. This is also seen in an experiment on a small scale flow lab.

Sammendrag

Denne oppgaven undersøker mulighetene for anti-slug regulering i offshore oljeproduksjon ved å benytte en reguleringsventil på havbunnen. En forenklet modell av et brønn-rørleding-riser system er introdusert og tilpasset en referansemodell av systemet i flytsimulatoren OLGA. Modellene har to frihetsgrader, en undervannsventil ved brønnhodet og en ventil ved overflaten. Dynamikken disse ventilene har på den forenklede modellen er tilpasset simuleringsdata fra OLGA ved bruk av bifurkasjonsdiagrammer.

En inngang-utgang kontrollérbarhetsanalyse av den forenklede modellen viser at anti-slug regulering ved bruk av undervannsventilen ved brønnhodet er vanskeligere en den vanlige løsningen, som er å bruke ventilen på overflaten. Dette er bekreftet ved å utføre simuleringer på den forenklede modellen ved bruk av $\mathcal{H}_\infty$-regulatorer.

Stabiliserende regulering av OLGA-modellen ved bruk av undervannsventilen var mislykket, selv om testingen ble utført ved å bruke flere forskjellige målekombinasjoner. En mer lovende løsning for å regulere riser slugging ved bruk av en undervannsventil er testet i OLGA, der ventilen er plassert nærmere bunnen av riseren. Dette er også observert i et experiment gjort på en mindre strømningslab.

Contents

Table of abbreviations

RHP	Right half-plane
LHP	Left half-plane
SISO	Single Input Single Output
MIMO	Multiple Input Multiple Output

Part I

1 Introduction

In offshore oil production, oil, water and gas are typically produced from several oil wells which are joined together to a common pipeline. It is then transported through the pipeline along the seabed and up a riser to a surface facility, such as an oil rig.

Slugging is a phenomenon that can occur with multiphase flow in pipelines, which is characterized by a series of liquid slugs separated by gas pockets. A particular type of slugging known as *riser slugging* may occur in a pipeline-riser system, usually due to a change in the oil reservoir conditions, such as a drop in pressure. Riser slugging is unwanted as it may cause wear and tear on equipment and the uneven flow can cause problems at the surface facilities.

A common solution to prevent riser slugging is to use a choke valve located topside, and reduce the flow. This will increase the pressure in the pipeline and consequently stop the slugging. However, this solution is undesirable as it will also reduce the production rate. A solution that can stabilize the flow without the loss in production is preferable, and in recent years active control of the topside choke valve have been successfully used to remove riser slugging.

A subsea valve located at the wellhead may also be used for control, and Statoil have reported use of such a valve for controlling slugging in the *well* [13]. However, this thesis is an investigation of the possibilities of using a subsea valve for riser slugging control. By using a model of a well-pipeline-riser in the advanced flow simulator OLGA as a test case, we want to find out if a subsea valve at can be used for control and which measurements may be suitable for use in an anti-slug controller.

1.1 Thesis outline

The objective of this thesis is to investigate the possibilities of anti-slug control using a subsea choke valve in a well-pipeline-riser system, where the subsea valve is located at the wellhead. The thesis consists of three parts, where the first part contains an introduction to the riser slugging problem and a presentation of the models used in the work. An advanced well-pipeline-riser model in the software OLGA is treated as the test system, and a simplified low order model of a well-pipeline-riser system is used for the analysis. The analysis will be done on the inputs and outputs of the system (the valves and available measurements), so

the simplified model is fitted to behave like the OLGA-model. This is verified using bifurcation diagrams.

The second part contains the theoretical background for the analysis done on the simplified model, where the objective is to find out which of the measurements are suitable for being used as *controlled variables* (CVs) in a control system. The analysis is based on *input-output controllability* where bounds are calculated on closed-loop transfer functions for different candidate CVs. The second part also includes a presentation of $\mathcal{H}_\infty$ control theory which have been used in the analysis, and also later used for control.

The last part of the thesis contains simulation results where some of the CVs found in part two are tested on both the simplified model and the OLGA-model. A new control structure is also proposed where the subsea valve is relocated near the inlet of the riser.

1.2 Slugging

Multiphase flow in pipes will behave differently depending on flow conditions like liquid-to-gas ratio, fluid properties, phase velocities, pipe inclination and pressure. These different types of flow may be categorized into flow regimes, where each regime has a different behavior. Figure 1.1 from [1] show examples of different flow regimes for both horizontal and vertical pipes.

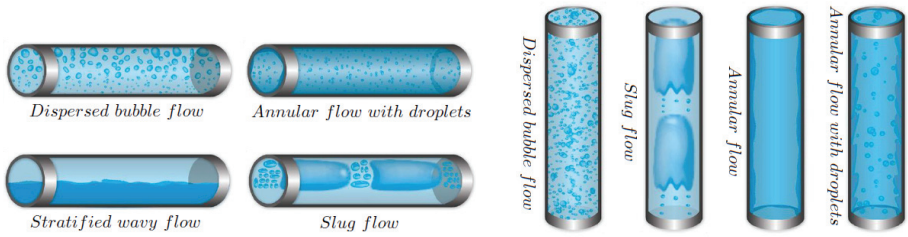

(a) Horizontal flow (b) Vertical flow

Figure 1.1: Illustration of flow regimes [1]

There are different types of slug flow, the most common being *hydrodynamic* slug flow. With stratified flow in a horizontal pipeline, this type of flow can occur when an increase in gas velocity causes waves to form. When the waves become so high that they reach the top of the pipe, they will block the gas flow.

The length of hydrodynamic slugs are usually relatively short, around 500 pipe diameters[1].

Terrain slugging can occur when the pipe has a low-point, as illustrated in figure 1.2. When the liquid in the low-point blocks the gas flow, the gas pressure will build up behind it. As the pressure increases, it will eventually match the hydrostatic pressure caused by the liquid column and start to push the liquid out. As the liquid leaves the pipe, it gets easier for the gas to push the liquid, and the liquid slug will flow out at a high velocity.

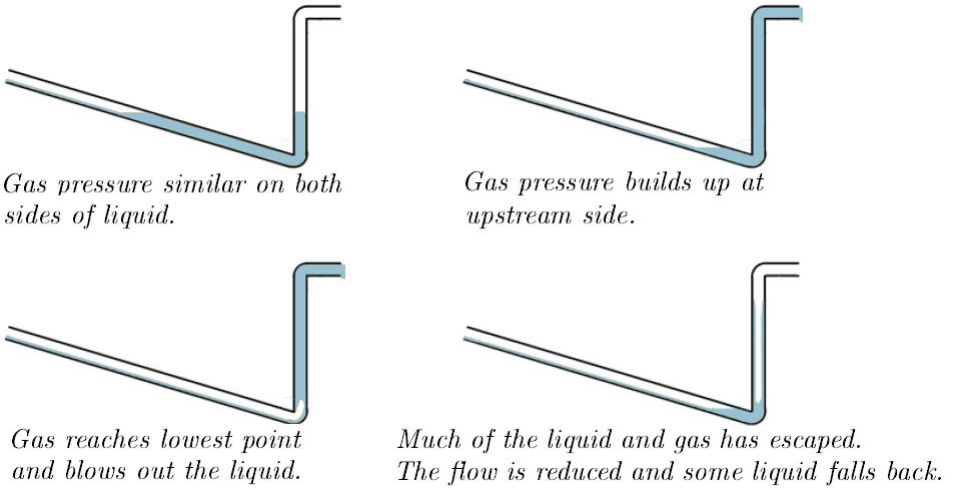

Figure 1.2: Terrain slugging cycle [1]

1.3 Riser slugging

Riser slugging is based on the same principle as for terrain-slugging. If the seabed upstream the riser has a downward slope, this will create a low-point in the pipeline at the bottom of the riser. If oil and water blocks the inlet to the riser, this can initiate a slug which grows upward the riser and back through the pipeline[16]. This is a known problem in the oil production industry and can happen due to changes in the well conditions, such as a declining well pressure in mature fields.

1.3.1 Problems caused by riser slugging

Riser slugging can have time periods of several hours, and this may cause large variations in pressure, temperature and flow rates. As a result of this, several problems are associated with slugging.

Wear and tear

The variations in pressure and flow during riser slugging may cause mechanical wear on the pipe and measurement equipment.

Flooding

The first stage in oil production at the surface facilities is separation of oil, gas, water and solids, which is done in separation tanks. When periods of high liquid flow caused by slugging enter these tanks, this may cause the separator tank to flood or lead to poor separation.

Hydrates

Hydrates are solid crystalline compounds of small gas molecules and water, and can form at high pressures and low temperatures. As oil wells produce water in addition to oil and gas, hydrate formation can throttle or completely plug the pipeline. Under periods of low liquid flow from the pipeline during riser slugging, the outflow contains more gas than usual. Gas has lower heat capacity than liquids, and a reduction in temperature causes hydrates to form more easily[1].

1.3.2 Solutions

A common solution to remove riser slugging, is to close a choke valve on top of the riser. A smaller valve opening will increase the system pressure and stabilize the flow.

A bifurcation diagram from [12] obtained by simulations on a model illustrates this, see figure 1.3. The figure show the oil mass flow rate as a function of the outlet valve opening.

The blue line represents the average production of oil in the system. When the valve opening reaches about 15% the system becomes unstable, i.e. slugging, and the black lines represent the maximum and minimum of the variations in the mass flow rate. The dotted blue line in the center is the average production

under slugging conditions, and we see that it drops when the system becomes unstable.

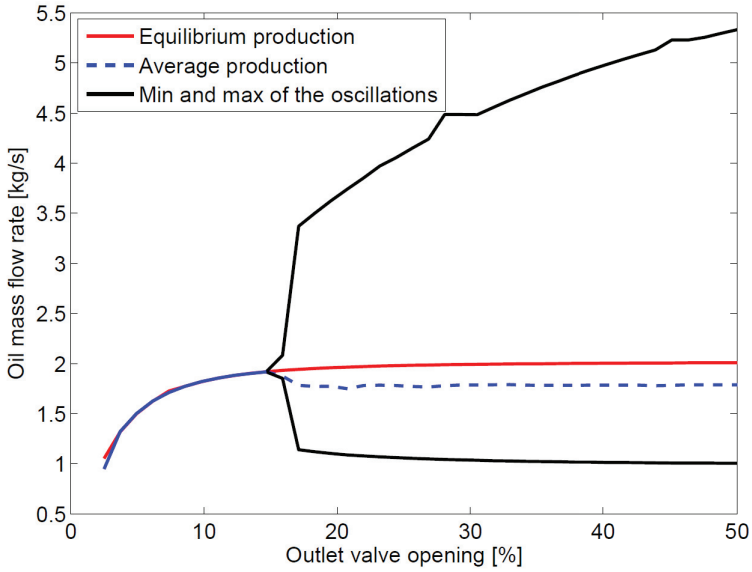

Figure 1.3: Bifurcation diagram di meglio

Active anti-slug control

Active control of a choke valve is a possible solution for stabilizing slug flow, and definition 1 from [16] formalizes this.

Definition 1. An anti-slug controller *is a controller the stabilizes a desired, non-oscillatory flow regime that exists at the same boundary conditions as riser slugging and thereby avoids the formation of riser slugging in the system.*

In figure 1.3, we see that by reaching this non-oscillatory flow regime (represented by the red line) using an anti-slug controller, the production rate can be kept at a higher level.

The conventional use of anti-slug control for stabilizing riser slugging is by use of the topside choke valve.

In the industry, there have been several reported uses of anti-slug control. A prototype control algorithm developed by ABB and BP have been started operating in the Hod field in the North sea[6], and Statoil have reported use of automatic slug control the Åsgard A production ship in the Norwegian sea[13].

In this thesis, however, we want to investigate the possibilities of using a subsea valve at the wellhead for controlling riser slugging.

2 Models

To study control of the riser slugging problem, two models are used in this thesis. An advanced model of the well-pipeline-riser system in OLGA is used as the test system, and a simplified 5-state model of the same system is used for analysis.

2.1 OLGA-model

OLGA is a commercial flow simulation software by SPT Group frequently used in the oil and gas industry[15]. The model is an expansion of an OLGA test system previously used for studying riser slugging in a pipeline-riser system, where the topside valve were used for control. Figure 2.1 show the well-pipeline-riser system, where a well has been added to get pressure driven inflow to the pipeline, and a subsea valve located at the top of the well is included as a new valve in the system.

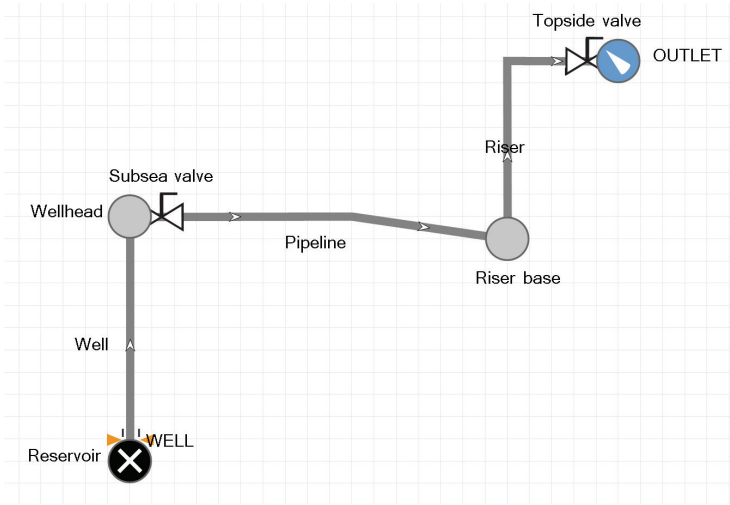

Figure 2.1: Well-pipeline-riser model in OLGA

The well is a 3.0 km long vertical pipe with a 0.12 m diameter. The pipeline has a length of 4.3 km and diameter of 0.12 m. The first 2.0 km section is horizontal, while the next section of 2.0 km has a vertical drop of 35 m. The last 300 m has a drop of 5 m, resulting in a low-point at the riser base. The

riser is a 300 m vertical pipe with a diameter of 0.10 m. A 100 m long horizontal pipe with diameter 0.1 m connect the riser with the topside valve.

With the subsea valve fully open, the model has a critical valve opening at 5 %, where the system changes from stable flow to unstable slug flow, as figure 2.2 demonstrates.

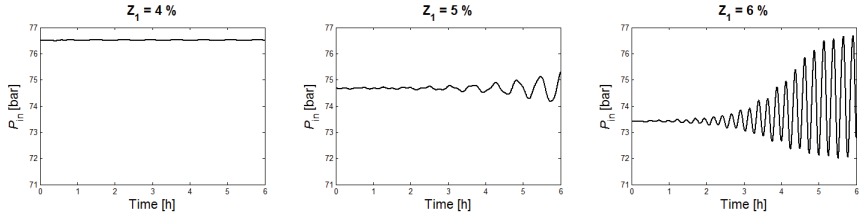

Figure 2.2: Simulations of OLGA case with increasing topside valve opening

2.2 Simplified 5-state model

2.2.1 Introduction

A simplified model of the well-pipeline-riser system used in this work is based on a 4-state model for a pipeline-riser system introduced in the article [7], where five other simple models for studying riser slugging are compared. To study the effect of pressure driven inflow, the model was later extended to a well-pipeline-riser model with 6 states, where the states were the gas and liquid masses in the three parts of the model.

The work in this thesis was started using the 6-state well-pipeline-riser model, but due to numerical problems under simulations, the model was modified. As two of the states showed similar dynamics, the gas and liquid masses in the well, it was decided to use just one state representing the total mass of the two phases in the well. Using only 5 states, the model show a dynamical behavior similar to the 6-state model, but without the numerical issues.

2.2.2 Model fundamentals

The five states of the model are:

$\dot{m}_{tw}$: Total mass of gas and liquid in the well
$\dot{m}_{gp}$: Mass of gas in the pipeline
$\dot{m}_{lp}$: Mass of liquid in the pipeline

$\dot{m}_{gr}$: Mass of gas in the riser
$\dot{m}_{lr}$: Mass of liquid in the riser

The state equations are the mass conservation for the well, pipeline and riser sections:

$$\dot{m}_{tw} = w_r - w_{wh} \tag{2.1}$$

$$\dot{m}_{gp} = w_{g,in} - w_{gr,b} \tag{2.2}$$

$$\dot{m}_{lp} = w_{l,in} - w_{lr,b} \tag{2.3}$$

$$\dot{m}_{gr} = w_{gr,b} - w_{g,out} \tag{2.4}$$

$$\dot{m}_{lr} = w_{lr,b} - w_{l,out} \tag{2.5}$$

where the subscripts g and l denotes gas and liquid phases and w_r is the mass flow from the reservoir. The flow rates in equations 2.1-2.5 are calculated by rest of the model equations given in Appendix A.

How the the riser slugging is modeled can be explained by looking at figures 2.3a and 2.3b. Figure 2.3a show the desired flow regime, where the liquid is uniformly distributed along the pipeline. Once the liquid level, h, reaches the height of the pipeline, h_c, liquid will block the gas flow into the riser, as illustrated in figure 2.3b.

The figure also show the locations of the available measurements which can be used by a controller, see table 1.

2.2.3 Fitting parameters

Six parameters are included in the model, used for fitting the simplified model to a desired system, K_1, K_2, K_g, K_l, K_w and K_h.

The system has two degrees of freedom, the subsea choke valve, Z_1, and the topside choke valve Z_2. They are both modeled as simplified valve equations with a linear valve characteristic, each with a fitting variable, K_1 and K_2:

$$w_{wh} = K_1 z_1 \sqrt{\rho_{mw,t}(P_{wh} - P_p)}$$

$$w_{out} = K_2 z_2 \sqrt{\rho_{mr,t}(P_{mr,t} - P_S)}$$

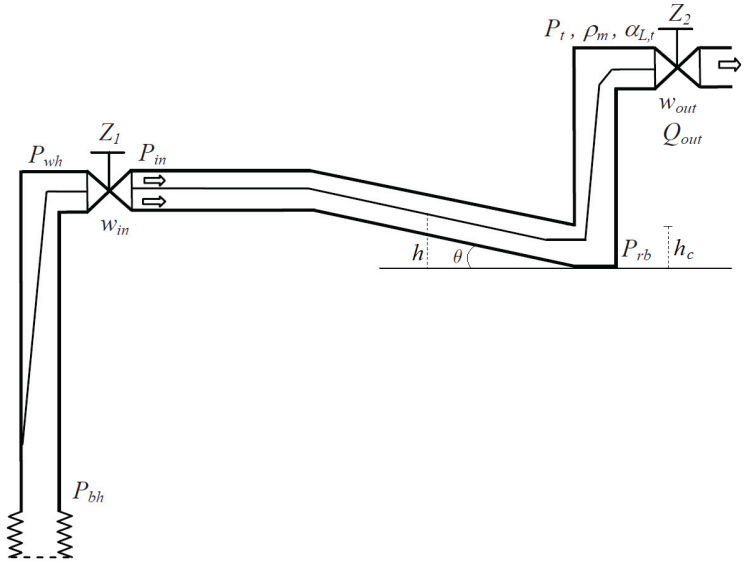

(a) Stable flow through the low-point

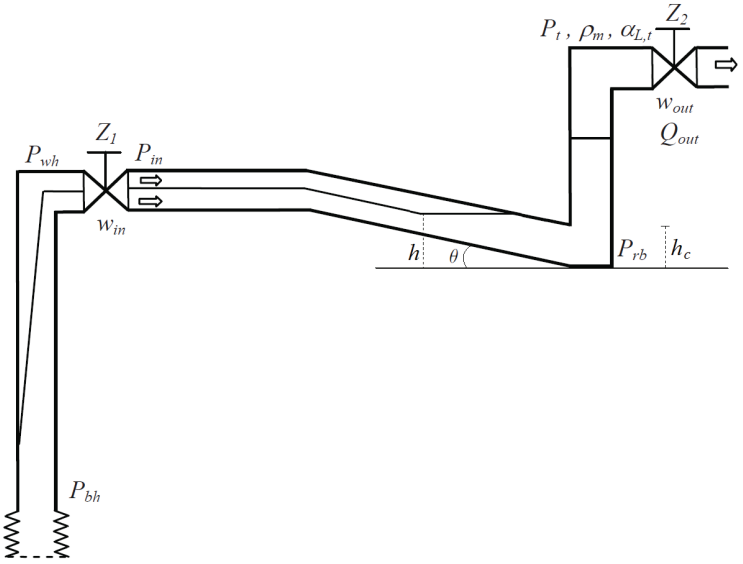

(b) Liquid blockage at the low point

Figure 2.3: Illustration of the simplified model

P_{bh}	pressure at bottom of well
P_{wh}	pressure at well-head
w_{in}	inlet mass flow rate to the pipeline
P_{in}	pressure at pipeline inlet
P_{rb}	pressure at riser base
DP_r	pressure drop over riser $(P_t - P_{rb})$
P_t	pressure at top of riser
Q_{out}	top-side choke volumetric flow rate
w_{out}	top-side choke mass flow rate
ρ_m	mixture density at top
$\alpha_{L,t}$	liquid volume fraction at top

Table 1: List of available measurements in the simplified 5-state model

The other fitting variables in the model are found in the following equations. The flow rate of gas through the low-point:

$$w_{gr,b} = K_g A_g \sqrt{\rho_{gp}(P_p - P_{r,b})}\; h < h_c$$

Liquid flow rate through the low-point:

$$w_{lr,b} = K_l A_l \sqrt{\rho_l (P_p + \rho_l g h - P_{r,b})}$$

Average gas mass fraction in the well:

$$\bar{\alpha}^m_{gw} = \frac{K_w \alpha^m_{gw,t}}{2}$$

Level of liquid at the low-point:

$$\bar{h} = K_h \bar{\alpha}_{lp} h_c$$

An explanation of these equations can be found with the rest of the model in appendix A.

These six tuning parameters are used to fine tune the simplified 5-state model so it will behave like the OLGA-model.

3 5-state model verification

For an analysis and controller design based on the 5-state model to be applicable to the OLGA-model, the two models should have a similar dynamical behavior. To see how the two valves affect the systems, bifurcation diagrams are made to compare the steady-state behavior, critical valve opening and the maximum and minimum of the oscillations. In addition, step responses from both valves are compared in both models.

3.1 Bifurcation diagrams

In a dynamical system, a *bifurcation* occurs when a small change in a parameter value will cause a fundamental change in the solutions to the system. A *bifurcation diagram* can be used to describe how the solutions behave as a function of a *bifurcation parameter*. Figure 3.1 show an example of a bifurcation diagram. When the bifurcation parameter reaches the bifurcation point, represented by the dotted line, the system goes from being stable to becoming oscillatory. The outer lines in the unstable region represents the maximum and minimum of the oscillations. In the unstable region, the center line represents the unstable steady-state solutions that exist here.

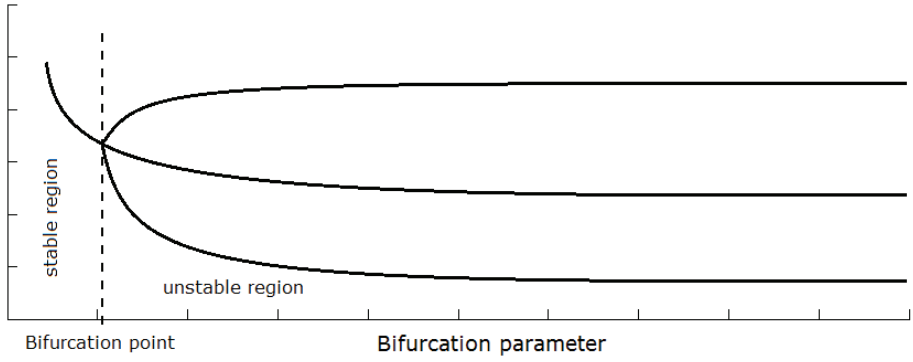

Figure 3.1: Bifurcation diagram explanation

Bifurcation diagrams were used to fit the behavior of the simplified model to the OLGA-model by tuning the fitting parameters presented in the previous chapter.

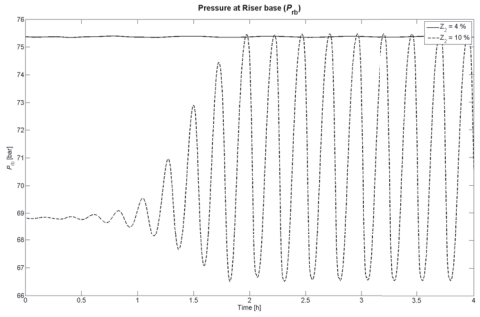

Figure 3.2: Example of two simulations done in OLGA for making the bifurcation diagrams

To illustrate how the bifurcation diagrams have been made, figure 3.2 show the pressure in the riser base for two simulations of the system using different valve openings. The solid line show the behavior in the stable region using a valve opening of 4%. The dotted line show the system when the valve opening have been increased to 10%, and the system have become unstable. By doing simulations for valve openings between 0 -100 %, and finding the maximum and minimum of the oscillations, one can plot this as a bifurcation diagram with the valve opening as the bifurcation parameter.

3.2 Fitting the model

The tuning variables in the 5-state model makes it possible to modify the 5-state model's dynamical behaviour to the OLGA-model. Bifurcation diagrams were first made by doing simulations on the OLGA-model, where both the subsea valve, z_1 and the topside valve, z_2 were used as bifurcation parameters. 17 simulations with increasing valve openings were performed, with most of the simulations done in the area with the most dynamics (from $0-20\%$). The steady-state values are obtained using the steady state pre-processor in OLGA, which calculates the steady-state and use this as initial values for the simulations[15].

The bifurcation diagrams using the simplified model were made in a similar manner as for the OLGA-model, where the model was implemented in the software Matlab[10].

There are two valves that can be used for control in the model, and this makes fitting both valves at the same time very time consuming, as the bifurcation diagrams have to be regenerated for every change in the parameters. Tuning

parameters that gave a satisfying fit were found by trial and error and insight in the model, see table 2.

Parameter	Value
k_a	0.904
k_h	0.600
K_g	0.030
K_o	0.236
K_1	0.014
K_2	0.011

Table 2: Tuning parameters used for fitting the simplified model to the OLGA model

3.3 Results

3.3.1 Bifurcation diagrams

All the measurements used for comparison are found in table 3 and the bifurcation diagrams of the three measurements P_{bh}, P_{in} and w_{out} are found in figure 3.3 and 3.4, the rest can be found in appendix B.

Figure 3.3 show the bifurcation diagrams made with the subsea valve z_1 as the bifurcation parameter, where the dotted red line represents the OLGA-model and the solid black lines are from the 5-state model. The diagrams using the topside valve z_2 as the bifurcation parameter are found in figure 3.4.

P_{bh}	Bottom hole pressure
P_{in}	Pressure at the pipeline inlet
P_t	Pressure at the top of the riser
w_{in}	Inlet mass flow
w_{out}	Outlet mass flow rate
Q_{out}	Outlet volumetric flow rate

Table 3: Variables used for bifurcation diagrams

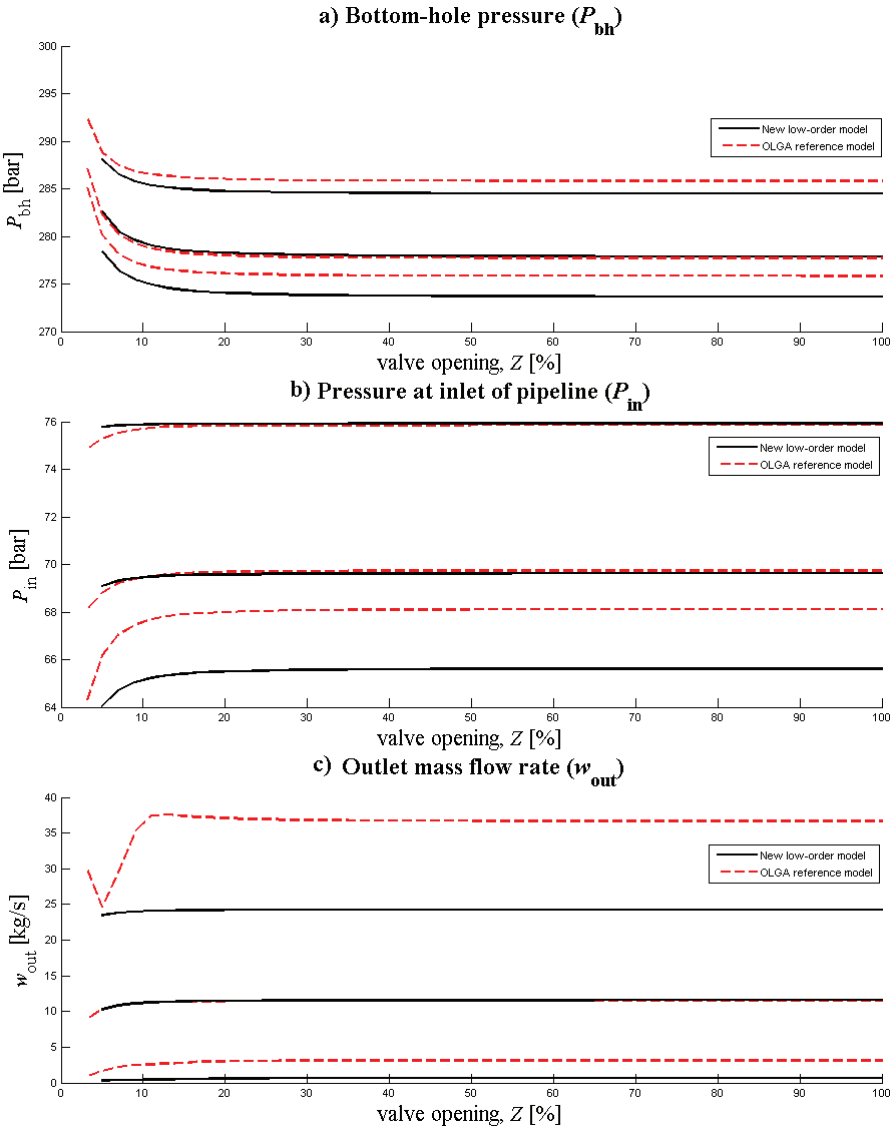

Figure 3.3: Bifurcation diagrams with the subsea valve z_1 as bifurcation parameter. The topside valve were kept constant at $z_2 = 30\%$.

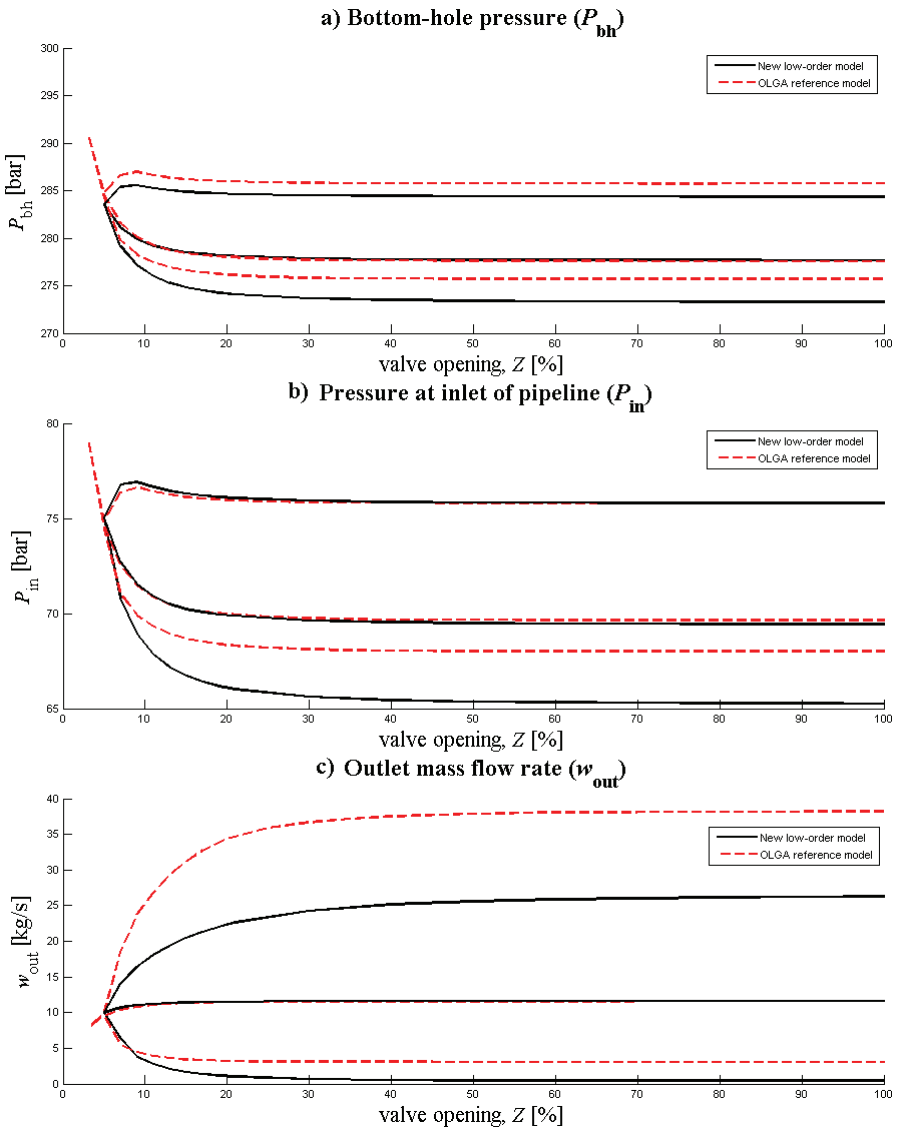

Figure 3.4: Bifurcation diagrams with the topside valve z_2 as bifurcation parameter. The subsea valve were kept constant at $z_1 = 100\%$.

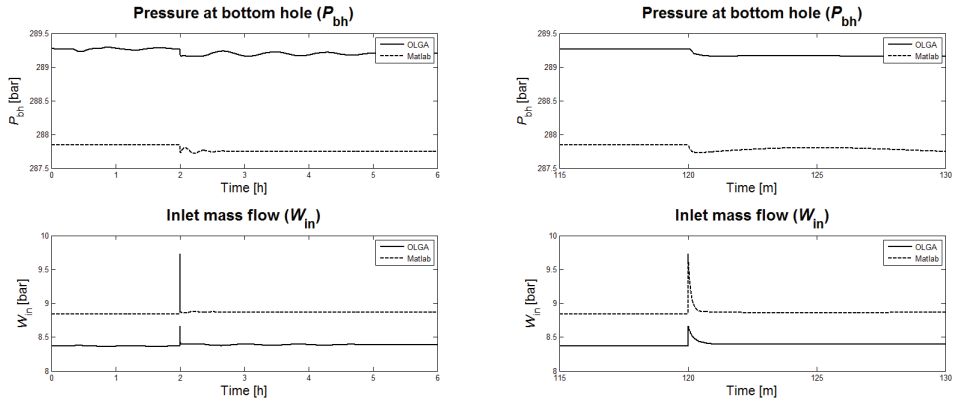

Figure 3.5: Step response comparison, subsea valve z_1

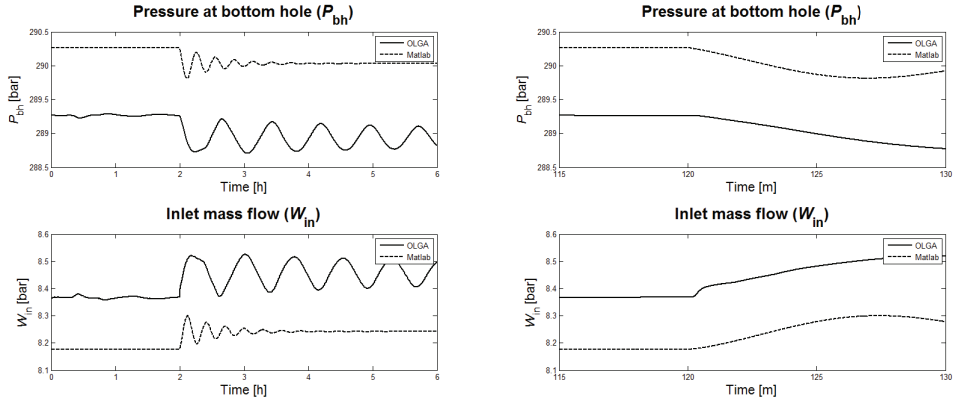

Figure 3.6: Step response comparison, topside valve z_2

3.3.2 Step response

The step responses of the simplified model compared to the OLGA-model is plotted in figure 3.5 and 3.6. For the subsea valve, z_1, the step is done from 10% to 11%, with the topside valve at $z_2 = 4\%$. A smaller step change was used for the topside valve, z_2, from 3.5% to 3.6% with the subsea valve at $z_1 = 10\%$.

Comments

The simplified model were fitted to the OLGA-model with emphasis on the steady-state behavior and critical valve opening. The maximum and minimum of the oscillations were of less importance as we want to use the model for control purposes where the anti-slug controller is used to stabilize these steady-state values.

We see from the bifurcation diagrams that the steady-state behavior of the simplified model was fitted very close to that of the OLGA-model for both valves in the system. The exception is P_t and Q_{out} using the subsea valve, and Q_{out} for the topside valve, where some offset is seen. These results can be found in appendix B.

The critical valve opening was also fitted very well using for the diagrams using the topside valve as bifurcation parameter. For the subsea valve the system were unstable for all valve openings and consequently there was no critical valve opening.

The step responses also look similar, but there is a small offset for all the variables. It is also clear that the oscillations in the OLGA-model have a longer time period than the simplified model, and they die out much slower.

Part II

4 Controllability analysis

To investigate which of the different measurements in the well-pipeline-riser system may be suitable for control, a controllability analysis is performed on the 5-state simplified model presented in 2.2. Note that here the term controllability refers to the *input-output controllability*, see definition 2 from [14], and not the state controllability often referred to in control theory.

Definition 2. (Input-output) controllability *is the ability to achieve acceptable control performance; that is, to keep the outputs (y) within specified bounds or displacements from their references (r), in spite of unknown but bounded variations, such as disturbances (d) and plant changes (including uncertainty), using available inputs (u) and available measurements (y_m or d_m).*

Input-output controllability is a property of the system, not the controller, and the purpose of the controllability analysis is to investigate how well a system can be controlled and which control structures should be used for control.

4.1 Theoretical background

The theory presented here is from Skogestad and Postlethwaite [14] and Storkaas [16].

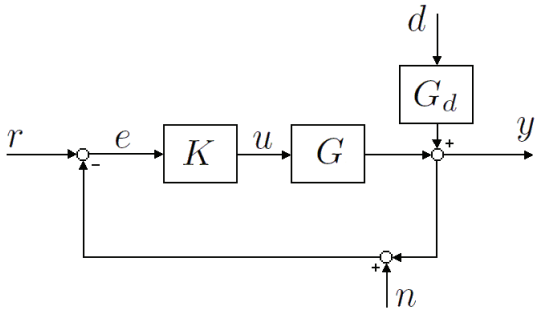

Figure 4.1: Classic feedback control structure

4.1.1 Transfer functions

Figure 4.1 show a basic feedback control setup where K is the controller, G is the system and G_d is the disturbance transfer function. The signals are the input r, error e, control signal u, noise n, disturbance d and output y.

Output signal

The control signal u can be written as

$$u = K(s)(r - y - n) \tag{4.1}$$

and the output y is

$$y = G(s)u + G_d(s)d \tag{4.2}$$

By substituting for u in 4.2, we get

$$y = G(s)K(s)(r - y - n) + G_d(s)d \tag{4.3}$$

and by solving for y

$$(I + GK)y = GKr + G_d d - GKn \tag{4.4}$$

we get the closed-loop system

$$y = (I + GK)^{-1}GKr + (I + GK)^{-1}G_d d - (I + GK)^{-1}GKn \tag{4.5}$$

We define $(I+GK)^{-1}$as the sensitivity transfer function S and $(I+GK)^{-1}GK$ as the complementary transfer function T, and get:

$$y = Tr + SG_d d - Tn \tag{4.6}$$

We see from equation 4.6 that T is the transfer function from the reference signal and measurement noise to the output, while S is the transfer function from the disturbance signal $G_d d$ to the output. Also note that $S + T = I$.

Control error

If we define the error e as $y - r$ and insert equation 4.6 for y, we get

$$e = y - r = Tr + SG_d d - Tn - r \tag{4.7}$$

and by using that $S + T = I$, we get

$$e = -Sr + SG_d d - Tn \tag{4.8}$$

Note that SG_d is the transfer function from the disturbance to the error signal.

Input signal

By taking the equation for the input signal

$$u = K(r - y) - Kn \tag{4.9}$$

and inserting the equation for the error signal and using $S + T = I$, we get

$$u = KSr - KSG_d d - KSn \tag{4.10}$$

Where KS and is the transfer function from the reference signal and measurement noise to the control signal and KSG_d is from the disturbance to the control signal.

4.1.2 Bounds on peaks of transfer functions

Bounds are calculated on the peaks of the transfer functions. The peak means the maximum value of the transfer function over the frequency response, called the $\mathcal{H}_\infty$-norm. The norm is defined as:

$$\|f(s)\|_\infty = \max_\omega |f(j\omega)| \tag{4.11}$$

The bounds presented here are from [16].

Bounds on S and T

We want S to be small to get a small control error for commands and disturbances.

The bound for the sensitivity function S depends on the distance between the RHP-poles and RHP-zeros. For a SISO system, the bound is found to be[14]:

For any RHP-zero z

$$\|S\|_\infty = M_S \geq \prod_{i=1}^{N_p} \frac{|z+p_i|}{|z-p_i|} \tag{4.12}$$

where N_p is the number of unstable poles p_i.

We want T to be small to avoid sensitivity to noise.

The bound for T is the same as the one for S [2], and for MIMO systems the bound is

$$M_{S,min} = M_{T,min} = \sqrt{1+\bar{\sigma}^2(Q_p^{-\frac{1}{2}} Q_{zp} Q_z^{-\frac{1}{2}})} \tag{4.13}$$

where

$$[Q_z]_{ij} = \frac{y_{z,i}^H y_{z,j}}{z_i + \bar{z}_j}, [Q_p]_{ij} = \frac{y_{p,i}^H y_{p,j}}{p_i + \bar{p}_j}, [Q_{zp}]_{ij} = \frac{y_{z,i}^H y_{p,j}}{z_i - p_j} \tag{4.14}$$

The vectors $y_{z,j}$ and $y_{p,i}$ are the unit output directions of the zeros z_i and poles p_i.

Bounds on SG and SG_d

SG should be small for reducing the effect of the input disturbances on the control error signal.

For any unstable zero in G

$$\|SG\|_\infty \geq |G_{ms}(z)| \cdot \prod_{i=1}^{N_p} \frac{|z+p_i|}{|z-p_i|} \tag{4.15}$$

The transfer function SG_d should be small to reduce the effect of general disturbances.

For any unstable zero in G_d

$$\|SG_d\|_\infty \geq |G_{d,ms}(z)| \cdot \prod_{i=1}^{N_p} \frac{|z+p_i|}{|z-p_i|} \tag{4.16}$$

where G_{ms} and $G_{d,ms}$ are the minimum phase stable versions of G and G_d, where both the RHP-pole and RHP-zeros are mirrored into the LHP:

$$G_{ms} \triangleq \prod_i \frac{s-p_i}{s+p_i} \cdot G(s) \cdot \prod_j \frac{s+z_j}{s-z_j} \tag{4.17}$$

Bounds on KS

KS should be small to avoid large input signals in response to noise and disturbances. In an unstable plant, a large value of KS can can cause saturation in u leading to difficulties in stabilization.

For multiple and complex poles p_i, a tight bound for KS is found by [3]:

$$\|KS\|_\infty \geq 1/\underline{\sigma}_H(\mathcal{U}(G)^*) \tag{4.18}$$

where $\underline{\sigma}_H$ denotes the lowest Hankel singular value and $\mathcal{U}(G)^*$ is the mirror image of the anti-stable part of G.

Bounds on KSG_d

KSG_d should be small to reduce the effect on the input by arbitrary disturbances.

A bound on KSG_d which is tight for multiple and complex unstable poles p_i

$$\|KSG_d\|_\infty \geq 1/\underline{\sigma}_H(\mathcal{U}(G_{d,ms}^{-1}G)^*) \tag{4.19}$$

4.1.3 $\mathcal{H}_\infty$-optimal control theory

$\mathcal{H}_\infty$-optimal control theory is a model based control design procedure where the controller design is formulated as an optimization problem. Due to the complex mathematics of the $\mathcal{H}_\infty$-methods, only a brief presentation is included here. For a more complete description the reader is referred to [14], [4].

The $\mathcal{H}_\infty$-optimization problem

When designing an $\mathcal{H}_\infty$-controller, it is useful to use a general control configuration, as seen in figure 4.2.

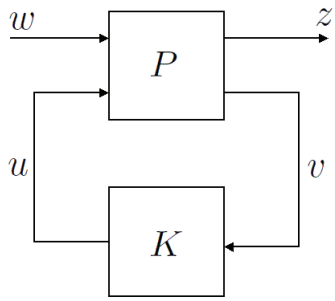

Figure 4.2: Generalized control configuration

In the generalized control configuration P is the generalized plant and K is the controller. The plant inputs are the signal w and the outputs z. v is the plants output used by the controller to calculate the control signal u. Note that the output z is the output signals of the plant which are to be minimized, e.g. the control error.

The generalized plant can be partitioned into the transfer function $P(s)$:

$$P(s) = \begin{bmatrix} P_{11}(s) & P_{12}(s) \\ P_{21}(s) & P_{22}(s) \end{bmatrix}$$

so that the parts are compatible with the signals in the generalized plant:

$$\begin{bmatrix} z \\ v \end{bmatrix} = P(s) \begin{bmatrix} w \\ u \end{bmatrix} = \begin{bmatrix} P_{11}(s) & P_{12}(s) \\ P_{21}(s) & P_{22}(s) \end{bmatrix} \begin{bmatrix} w \\ u \end{bmatrix}$$

$$u = K(s)v$$

Including the controller K gives the closed-loop transfer function from w to z:

$$\begin{aligned} z &= \left[P_{11} + P_{12}K(I - P_{22}K)^{-1}P_{21} \right] w \\ &= \mathcal{F}_l(P, K)w \end{aligned}$$

$\mathcal{F}_l(P, K)$ is called the *lower linear fractional transformation* (LFT) of P and K.

The $\mathcal{H}_\infty$ optimal control problem is to find all stabilizing controllers K which minimize the $\mathcal{H}_\infty$-norm of $\| \mathcal{F}_l(P, K) \|_\infty$, i.e.:

$$\min_K \| \mathcal{F}_l(P,K) \|_\infty$$

Mixed sensitivity

The bounds presented in chapter 4.1.2 consider the transfer functions one at a time. As an analysis based only on single transfer functions may give conflicting results, it is preferable to design a controller where combinations of transfer functions are considered.

We want to limit S for performance and disturbance rejection and T for noise attenuation and robustness. In [16] it was found that for a pipeline-riser system, avoiding input saturation is essential for stabilizing controllers, therefore we want to limit KS to control the input usage. This can be done by formulating an *S over KS over T* mixed sensitivity problem, where the three transfer functions are considered simultaneously. It can also be useful to specify *weights* on these transfer functions, and the LFT then becomes:

$$\mathcal{F}_l(P,K) = \begin{bmatrix} W_P S \\ W_u K S \\ W_T T \end{bmatrix} \tag{4.20}$$

where W_P, W_u and W_T are the weighting for the transfer functions. Figure 4.3 show a block diagram of a generalized control configuration where these weights are included.

For the well-pipeline-riser model, G is the well-pipeline-riser system and K is the anti-slug controller. The input w is the set-point to the anti-slug controller, and u is the input the to the valve. v is the CV used by the controller. $z_1$is the weighted control error, z_2 is the weighted input signal and z_3 is the weighted output signals.

4.1.4 Solving the optimization problem

Software for solving the the $\mathcal{H}_\infty$ optimization problem is available in Matlab, and the algorithm uses an iterative approach. Let γ_{min} be the minimum value for $\|\mathcal{F}_l(\mathrm{P,K})\|_\infty$ and given a $\gamma > \gamma_{min}$, a suboptimal control problem is to find all controllers K such that

$$\| \mathcal{F}_l(P,K) \|_\infty < \gamma$$

By decreasing this γ-value and performing the optimization iteratively, one can reach close to an optimal solution.

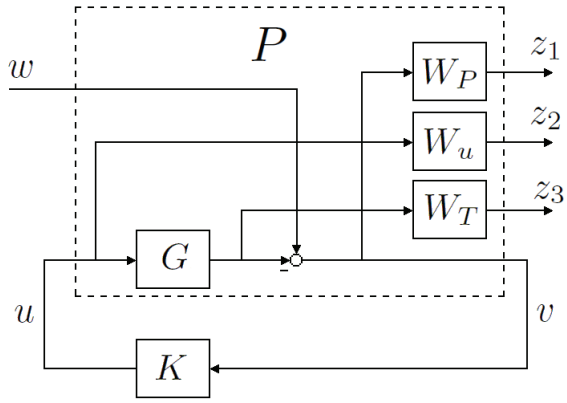

Figure 4.3: Mixed sensitivity

It is this γ-value which is used in the controllability analysis as a single measure to compare the different candidate CVs, where the transfer functions S, T and KS is taken into account. A lower γ-value means better controllability.

4.2 Procedure for calculating bounds and $\gamma - values$

All the available measurements in the well-pipeline-riser system are considered as candidate CVs in the controllability analysis, to see how they will perform in an anti-slug controller. In addition, some combinations of measurements are also considered as CVs.

For comparison purposes, the analysis is done for three different input configurations; using the subsea valve, using the topside valve, and using both valves together. Before doing the analysis, the model was linearized and scaled to ensure that all outputs are of about equal importance in terms of their magnitude.

Linearization

Due to fact that the controllability analysis presented here is using linear tools, the nonlinear 5-state model has to be linearized around the point in which one want to do the analysis. This linearization was done numerically in Matlab, and [14] specifies that to deal with slowly varying changes, the analysis may be performed at several operating points. The two operating points which the model was linearized around were $z_1 = 10\%$, $z_2 = 10\%$ and $z_1 = 30\%$, $z_2 = 10\%$.

Scaling of the system

A proper scaling of the system is necessary for the controllability analysis, and it makes the weight selection in the $\mathcal{H}_\infty$-controller design simpler. It is performed as outlined in [14].

The objective of the scaling is to make all the signals in the system less than one in magnitude. This way, one can compare different signals that originally is of different magnitude.

The inputs, z_1 and z_2, is scaled using the maximum allowed deviation from the nominal value of the valves, using the scaling factor:

$$D_u = \begin{bmatrix} \min(z_1, 1 - z_1) & 0 \\ 0 & \min(z_2, 1 - z_2) \end{bmatrix} \tag{4.21}$$

The disturbances modelled in the system are gas and liquid mass flow rates entering at the inlet of the pipeline, d_1 and d_2 respectively. Their maximum expected magnitude is around 5% of the nominal values of the inflow to the system, which for the gas is $w_{g,nom} = 0.36$ and the liquid $w_{l,nom} = 8.64$. The scaling of the disturbances then becomes:

$$D_d = \begin{bmatrix} 0.05 * 0.36 & 0 \\ 0 & 0.05 * 8.64 \end{bmatrix} \tag{4.22}$$

The scaling factors of the available measurements are given in tables 4, 5 and 6 in the results.

4.2.1 Calculating Bounds

The bounds of the transfer functions were calculated in Matlab. An example of how a bound have been calculated of the sensitivity function S, where the bottom hole pressure, P_{bh}, is used as a CV and the subsea valve, z_1, is used as control input, can be found in appendix C. All the Matlab-code used in thesis is available on the web page [11] and is written based on earlier work on a similar model in Jahanshahi[8].

4.2.2 $\mathcal{H}_\infty$ and the $\gamma - value$

$\mathcal{H}_\infty$-controllers were made in Matlab for the same candidate CVs as the bounds were calculated for, and a Matlab-script of how the controller is made using P_{bh} as a CV and z_1 as control input is found in appendix C. Note that although its only the γ-value of the different controllers that is used in the controllability

analysis, the controller itself are tested for some of the candidate CVs later in the report.

Weights in the mixed sensitivity $\mathcal{H}_\infty$-controller

To emphasize the minimization of S at low frequencies, a weight with integral action, W_{p2}, is used for the measurement actually tested as a CV, while a constant weight, W_{p1}, are used for the rest of the measurements. In the general control configuration in figure 4.3, this corresponds to using the weight W_{p2} for the CVs in the signal v, and the weight W_{p2} for the output z_1. This is to have the same cost function in all the tests for the measurement selection.

A constant weight, W_u, is used on the signals in KS for robustness and to restrict input usage.

For the complementary sensitivity function T, the weight W_T is chosen to limit the gain at high frequencies.

The weights used for the controller design is given in 4.23:

$$\begin{aligned} W_{p1} &= 0.5 \\ W_{p2} &= \frac{0.5s + 0.05}{s + 0.0005} \\ W_u &= 10 \\ W_T &= \frac{100s^2 + 20s + 1}{0.01s^2 + 0.2s + 1} \end{aligned} \tag{4.23}$$

To get comparable results for the different measurements, the same weights are used for all the configurations tested.

4.3 Results

The results from controllability analysis done around the operating point $z_1 = 10\%$ and $z_2 = 10\%$ are found in tables 4, 5 and 6, where the analysis is done using the subsea valve, topside valve and both valves together. The tables present for every candidate CV: the value in the operating point, scaling factor D_y, steady-state gain $G(0)$, the bounds on the transfer function and the $\gamma - value$.

Measurement	Value	D_y	$G(0)$	$\|S\| = \|T\|$	$\|KS\|$	$\|SG\|$	$\|KSG_{d1}\|$	$\|KSG_{d2}\|$	$\|SG_{d1}\|$	$\|SG_{d2}\|$	γ
P_{bh}	280.70	1	-2.299	3.23	1.39	5.61	0.21	0.46	0.24	0.51	50
P_{wh}	71.91	1	-1.403	2.38	1.42	2.51	0.21	0.46	0.18	0.40	48
W_{in}	10.81	1	0.632	7.35	4.79	9.02	0.21	0.46	0.22	0.46	132
P_{in}	70.92	1	0.452	1	1.35	0	0.21	0.46	0	0	59
P_{rb}	68.70	1	0.197	1.43	1.14	2.33	0.20	0.55	0.03	0.26	86
DP_r	16.77	1	-0.018	1.02	0.85	0.29	0.16	0.46	0.29	0.23	100
P_t	51.93	1	0.215	1.84	1.92	0.75	0.15	0.55	0.08	0.24	84
Q_{out}	19.92	2	0.589	1.77	0.75	3.70	0.21	0.54	0.26	0.53	49
W_{out}	10.81	1	0.632	1.91	0.57	2.65	0.15	0.58	0.22	0.90	47
ρ_t	542.58	50	-0.007	2.28	1.06	1.77	0.23	0.68	0.25	0.67	100
$\alpha_{L,t}$	0.63	1	-0.001	2.29	16.70	0.11	0.23	0.68	0.02	0.04	554
$P_{bh}P_{wh}$				1	1.00	0	0.11	0.23	0	0	37
$P_{bh}W_{in}$				1	1.34	0	0.11	0.23	0	0	48
$P_{bh}P_{in}$				1	0.97	0	0.11	0.23	0	0	36
$P_{wh}W_{in}$				1	1.36	0	0.11	0.23	0	0	46
$P_{wh}P_{in}$				1	0.98	0	0.11	0.23	0	0	35
$W_{in}P_{in}$				1	1.30	0	0.11	0.23	0	0	59

Table 4: Results from the controllability analysis using the subsea valve z_1 as input.

The last three columns in table 6 for the MIMO results show the γ-values from the $\mathcal{H}_\infty$-analysis using integral action on the first measurement, second measurement and both measurements respectively.

Comments

From the results of the controllability analysis for the subsea valve z_1, we see that:

- All the minimum achievable peaks for $|S|$ using a single controlled variable is higher than 1, except for the inlet pressure, P_{in}.
- The bottom hole pressure, P_{bh}, shows the largest steady state gain ($G(0)$).
- By looking at the γ-values, the pressures P_{bh}, P_{wh} and the mass and volumetric flow out of the system W_{out} and Q_{out} looks as they are the most promising controlled variables.

Measurement	Value	D_y	$G(0)$	$\|S\| = \|T\|$	$\|KS\|$	$\|SG\|$	$\|KSG_{d1}\|$	$\|KSG_{d2}\|$	$\|SG_{d1}\|$	$\|SG_{d2}\|$	γ
P_{bh}	280.70	1	-2.97	1	0.46	0	0.071	0.151	0	0	20
P_{wh}	71.91	1	-2.91	1	0.47	0	0.071	0.151	0	0	20
W_{in}	10.81	1	0.82	1	1.59	0	0.071	0.151	0	0	60
P_{in}	70.92	1	-3.06	1	0.45	0	0.071	0.151	0	0	19
P_{rb}	68.70	1	-3.38	1	0.38	0	0.068	0.183	0	0	16
DP_r	16.77	1	-0.02	1	0.28	0	0.052	0.153	0	0	100
P_t	51.93	1	-3.36	2.54	0.64	4.64	0.051	0.183	0.085	0.312	38
Q_{out}	19.92	2	0.85	1	0.25	0	0.071	0.178	0	0	37
W_{out}	10.81	1	0.82	1	0.19	0	0.051	0.192	0	0	39
ρ_t	542.58	50	-0.10	2.29	0.35	5.73	0.076	0.228	0.244	0.688	96
$\alpha_{L,t}$	0.63	1	-0.01	2.29	5.55	0.36	0.076	0.228	0.016	0.044	242
$P_{in}P_t$				1	0.37	0	0.033	0.085	0	0	14
$P_{in}W_{out}$				1	0.17	0	0.033	0.088	0	0	11
P_tW_{out}				1	0.17	0	0.033	0.088	0	0	16
$P_t\rho_m$				1	0.18	0	0.025	0.094	0	0	20
$P_{bh}W_{out}$				1	0.31	0	0.037	0.111	0	0	11

Table 5: Results from the controllability analysis using the topside valve z_2 as input.

Measurement	$\|S\| = \|T\|$	$\|KS\|$	$\|SG\|$	$\|KSG_{d1}\|$	$\|KSG_{d2}\|$	$\|SG_{d1}\|$	$\|SG_{d2}\|$	γ_1	γ_2	γ_3
$P_{bh}P_{in}$	1	0.25	0	0.025	0.054	0	0	10	10	14
$P_{bh}P_{rb}$	1.01	0.22	0.01	0.026	0.056	0.003	0.005	10	9	15
$P_{bh}P_t$	1.34	0.26	3.61	0.028	0.066	0.181	0.516	10	16	19
$P_{bh}W_{out}$	1.10	0.15	0.07	0.028	0.070	0.040	0.285	9	30	100
$P_{wh}P_{rb}$	1.02	0.23	0.23	0.026	0.056	0.009	0.042	9	9	24
$P_{wh}P_t$	1.33	0.27	3.16	0.028	0.066	0.193	0.515	10	16	25
$P_{wh}W_{out}$	1.33	0.15	0.33	0.028	0.070	0.055	0.457	6	30	60
$P_{in}P_t$	1	0.26	0	0.028	0.066	0	0	10	16	89

Table 6: Results from the controllability analysis using both valves as input.

- The inlet mass flow, W_{in} has a large value for the bound on $|S|$ and consequently a large γ-value.
- When using two measurements, the combinations of P_{bh} & P_{in} and P_{wh} & P_{in} have the lowest γ-values.
- Comparing the results of the subsea valve with the topside valve, we see that the $\gamma - values$ are generally higher using the subsea valve, and the gain is lower for all the variables. This indicates that the subsea valve is not as good as the topside valve when used for controlling riser slugging.

Part III

5 Simulations

5.1 Introduction

To test the possibilities of anti-slug control using the subsea valve, the most promising CVs from the controllability analysis in chapter 4.3 are tested in simulations on both the simplified model and the OLGA-model. The $\mathcal{H}_\infty$-controllers developed in section 4.2 are used for control of the simplified model using Simulink in Matlab. In OLGA, the standard PID controllers included in the software were used.

The objective of the anti-slug controller is to keep the flow stabile at the same boundary conditions that would give riser slugging without control. To start a controller while the system is slugging may be difficult, so the simulation tests in this thesis are done with the system starting at an unstable equilibrium point with the controller on from the start. In a real process, a start-up procedure of an anti-slug controller can be to first choke a valve until the system is stable, and activate the controller. Then the system can brought to the desired operating point by changing the setpoint of the controller[16].

5.2 Simulations on the simplified 5-state model

The simplified model of the well-pipeline-riser system was simulated using Simulink where the model was was implemented using an S-function, a tool for using a Simulink-block written in Matlab-code. Figure 5.1 show a screenshot from the program, where the bottom hole pressure P_{bh} is tested as a CV. The $\mathcal{H}_\infty$-controller made in section 4.2 were implemented as a state-space block.

5.2.1 Disturbances

The different CVs are tested by their ability to counteract disturbances. Two disturbances are used in the test, d_1 and d_2, which are mass flow rates of gas and liquid entering at the inlet of the pipeline, see equations 5.1 and 5.2. The tests were done by first simulating the system using disturbances with a magnitude of 1% of the nominal value of mass flow into the system. Then, simulations were done with increasing magnitude, until the controller were no longer able to keep the system stable. The maximum magnitude tested were 5%.

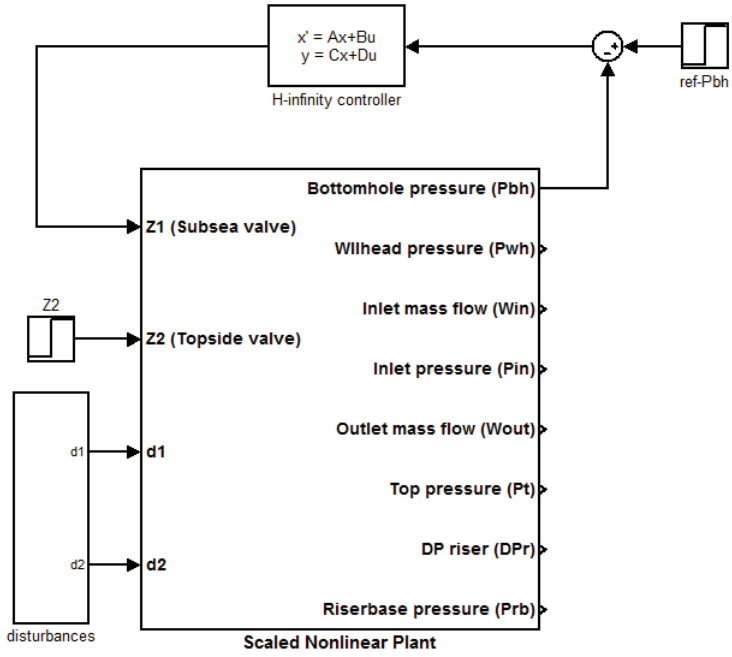

Figure 5.1: The simplified model simulated in Simulink. The example show the bottom hole pressure P_{bh} used as a CV and the subsea valve z_1 used as input.

$$w_{g,in} = w_{wh}\alpha^m_{gw,t} + d_1 \tag{5.1}$$

$$w_{l,in} = w_{wh}(1 - \alpha^m_{gw,t}) + d_2, \tag{5.2}$$

where w_{wh} is the wellhead flow rate and $\alpha^m_{gw,t}$ is the total gas mass fraction in the well.

To be able to compare the performance of the controller using different CVs, it is the scaled model that have been used in the simulations. Note that the size of the disturbances are done in the scaling of the system, so the magnitude of the disturbances are always 1 in the simulations. Using this scaling, a requirement for acceptable performance is that for any disturbance between -1 and 1

entering the system, the controller should keep the outputs between -1 and 1 by using an input within -1 and 1.

The system was first tested using single measurements as a CV, then a combinations of measurements as a CV and finally some simulations were done using both valves together by a MIMO controller.

5.2.2 SISO control - using a single measurement for control

The CVs tested using SISO control were: P_{wh}, P_{bh}, P_{rb} and W_{out}.

P_{wh} - Pressure at wellhead Figure 5.2 show the simulation using P_{wh} as CV. The top left corner show the input used and the top right corner show the steps in the disturbances. The system were able to handle disturbances up to 2%.

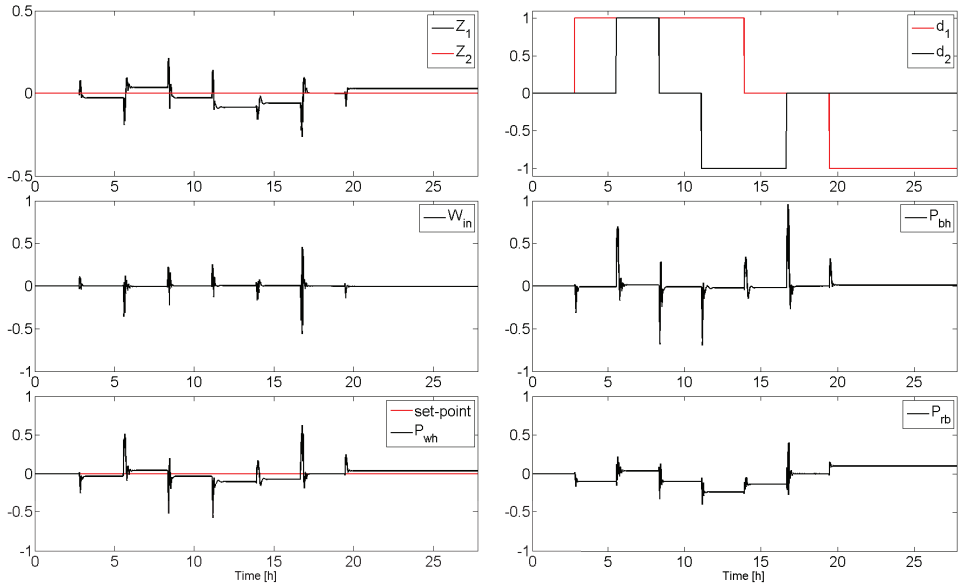

Figure 5.2: Control of system using P_{wh} as controlled variable

P_{bh} - Bottom hole pressure When using the bottom hole pressure P_{bh} as controlled variable, the system were kept stable with disturbances at 1%, but

when increasing to 2% the controller were no longer able to keep the system stable. The simulations is shown in figure 5.3.

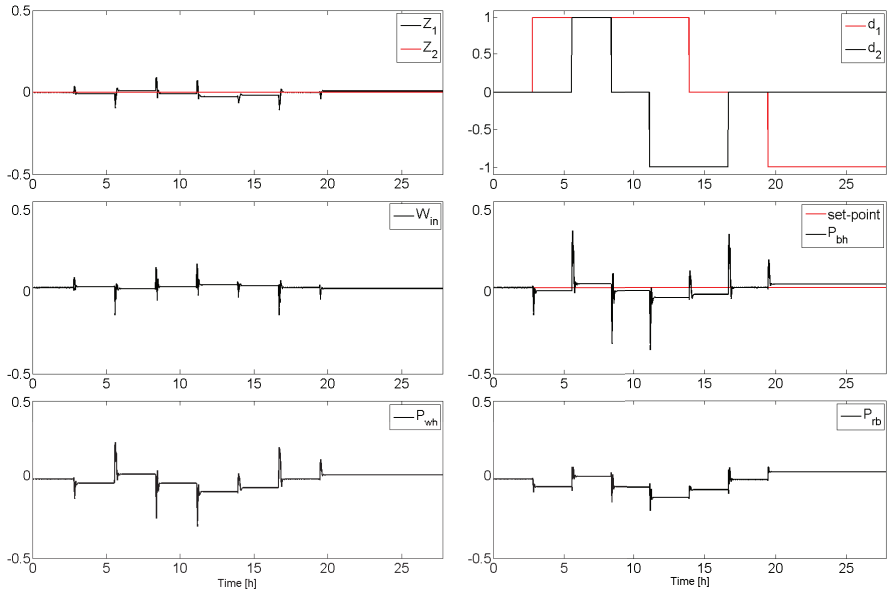

Figure 5.3: Control of system using P_{bh} as controlled variable

Outlet mass flow W_{out} and riser base pressure P_{rb} The outlet mass flow W_{out} did get the smallest γ-value in the controllability analysis, but during simulations the controller was unable to keep this system stable even at 1% disturbances. The riser base pressure P_{rb} was also tested as a CV, and the controller did manage to keep the system stable with 1% disturbances, but the response to the disturbances was very oscillatory. These simulations can be seen in appendix E.2.

5.2.3 MISO control - Using a combination of measurements

The γ-values from the controllability analysis suggest that using a combination of measurements will slightly enhance the performance of the controller. The combinations tested were: P_{bh} and P_{in}, P_{bh} and W_{in}, P_{wh} and W_{in}.

The reason for choosing combinations including W_{in} is that although this variable did not give good results in the controllability analysis, it may be suitable as the CV in an inner loop using cascade control in OLGA.

Bottom hole pressure P_{bh} and P_{in} A combination of P_{bh} and P_{in} were able to stabilize the slugging with disturbances up to 3%. However, with these disturbances the bottom hole pressure P_{bh} would give large peaks, above 1 in the scaled model, see figure 5.4.

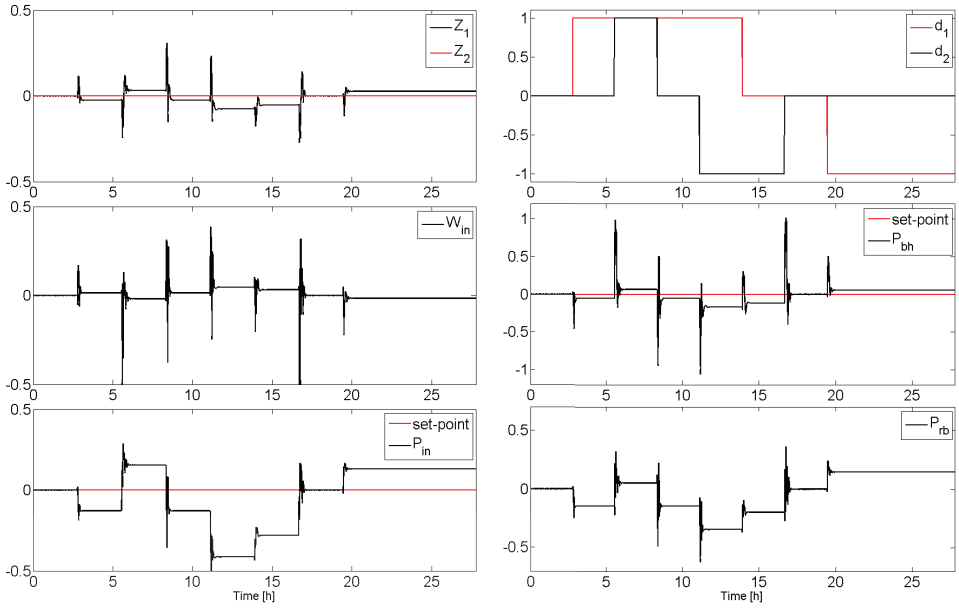

Figure 5.4: Stabilizing control of the system using a combination of P_{bh} and P_{in} as controlled variables. 3 % disturbance

Combinations using inlet mass flow rate The combinations tested with a pressure measurement combined with inlet mass flow, P_{bh} and W_{in}, and P_{bh} and W_{in}, were not able to improve the performance further from using a single measurement. Neither of the two combinations were able to keep the flow stable with disturbances larger than 1%. The results can be found in appendix E.2.

5.2.4 MIMO control - Using both valves for control

The model was also tested using both valves with a combination of two measurements: P_{in} and P_t , P_{bh} and P_{in} , P_{wh} and P_{rb}. All the combinations tested were able to keep the flow stable with 5 % disturbances.

Stabilizing control of the nonlinear system using both the subsea and the topside valve using a combination of P_{bh} and P_{in} as CVs are shown in figure 5.5.

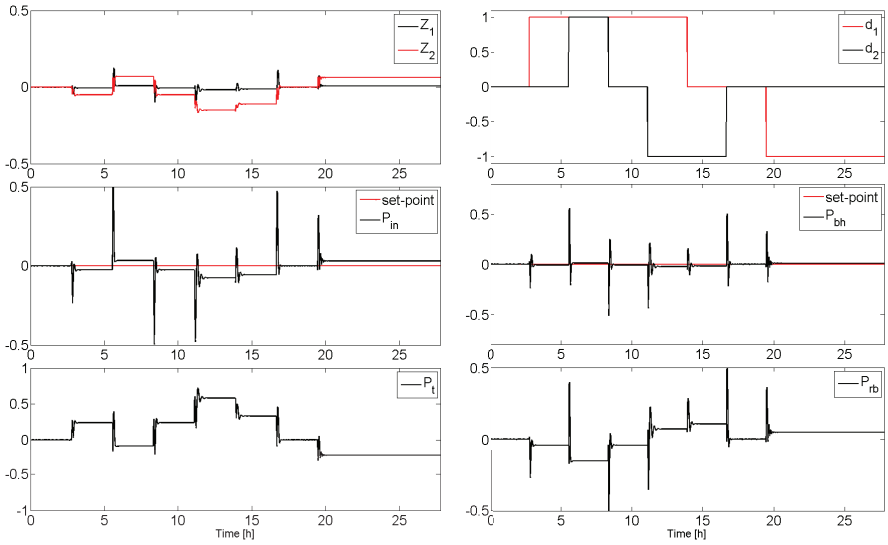

Figure 5.5: Control of nonlinear model using both valves and P_{bh} and P_{in} as controlled variables

5.2.5 Summary of the simulations on the simplified model

From the simulations of the nonlinear model, we found that the controller will only counteract small disturbances around the linearization point when using the subsea valve. The controller is designed using a linearized model, and the disturbances will move the system away from the linear region. The controller was therefore very unrobust when used with the highly nonlinear model.

During the $\mathcal{H}_\infty$-controller design, it was noted that a higher weight on low frequencies of the sensitivity function S (i.e. more integral action) would help

stabilizing the system. This is most likely due to the fact that the controller then will keep the system closer to the linearization point.

It was also found in the simulations that the disturbance the controller had most problems with was an increase in d_2, the liquid mass flow rate.

The controller worked better using both valves in a MIMO scheme, and this is probably due to the fact that the topside valve is doing most of the stabilising control.

5.3 OLGA-simulations

Stabilizing the riser slugging in OLGA using the subsea valve did not work, despite extenstive testing of control structures and PID-tuning. All the measurements and measuement combinations that were tested are shown in table 7. Altough the variations in pressure were slighty smaller when using control than they were in open-loop, the system was still unstable. The lack of gain the valve had on the CVs often made the valve go into saturation.

Measurement	Description	OLGA setup
P_{bh}	SISO control using bottom hole pressure	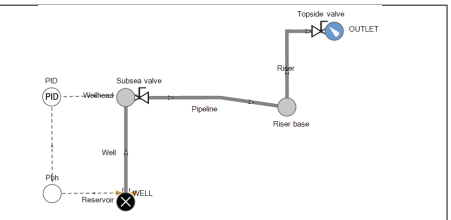
P_{wh}	SISO control using wellhead pressure	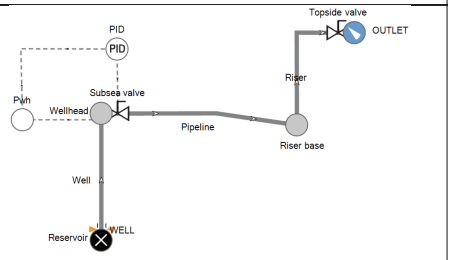
P_{bh} and P_{wh}	Cascade control with P_{bh} in outer loop and P_{wh} in inner loop	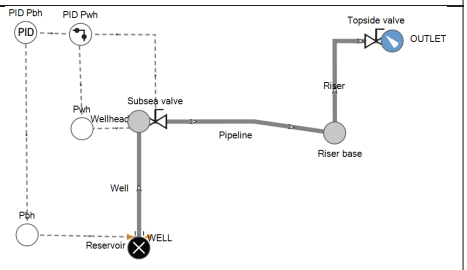
P_{bh} and W_{in}	Cascade control P_{bh} in outer loop and inlet mass flow W_{in} in inner loop	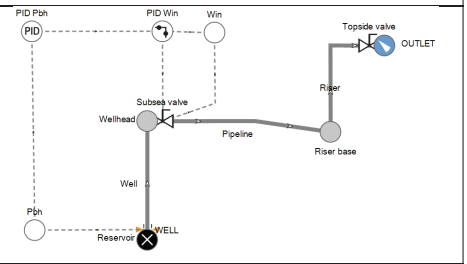
P_{wh} and W_{in}	Cascade control P_{wh} in outer loop and inlet mass flow W_{in} in inner loop	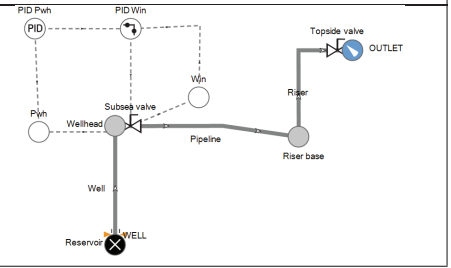

Table 7: Control structures tested in OLGA using PID-controllers

6 Subsea valve closer to riser base

As we were unable to control riser slugging in OLGA using the subsea valve located at the wellhead, an attempt of using a subsea valve closer to the riser base for stabilizing control was done. The OLGA-model were modified by moving the subsea valve from the wellhead to the riser base, as seen in figure 6.1. In theory, this should be a better solution, as the valve is closer to the origin of the instability, but a subsea valve located this close to the riser base is a more unlikely scenario in real systems. However, if several oil wells are connected to be transported through a pipeline not far from the riser, a valve could be placed in this position.

Using a subsea valve at the riser base for slugging control were briefly tested in OLGA, and results from an experiment done on a small scale flow flow rig with a similar setup is presented.

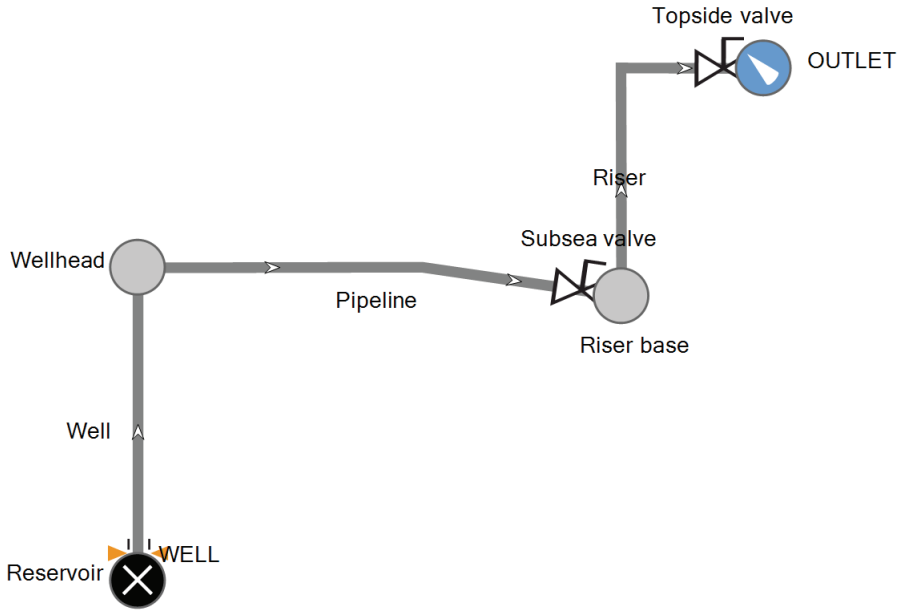

Figure 6.1: Diagram of the well-pipeline-riser model with the subsea valve moved to the riser base.

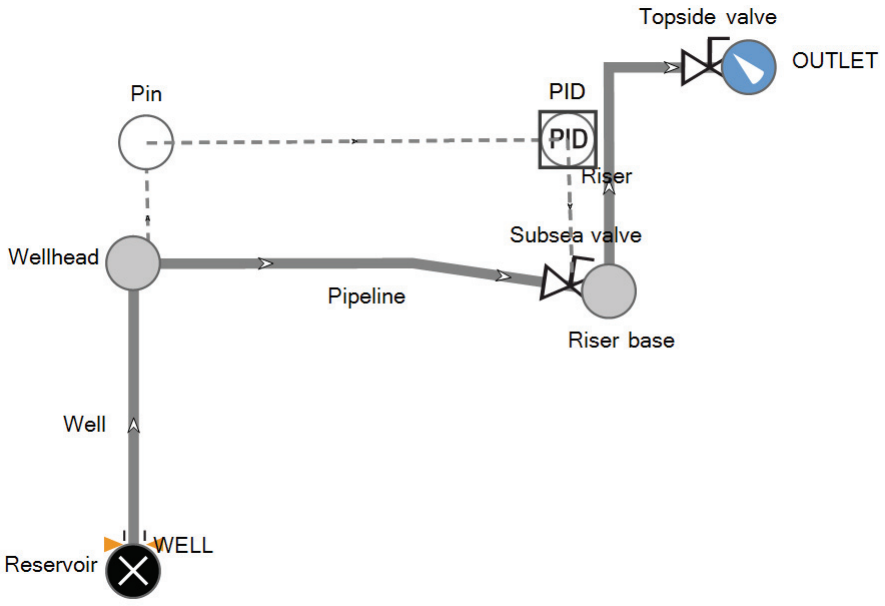

Figure 6.2: PI control of the well-pipeline-riser system using subsea valve located at riser base

6.1 OLGA simulation

Using the relocated subsea valve and a PID-controller with feedback measurement from the inlet pressure P_{in}, the well-pipeline-riser system was simulated in OLGA. Figure 6.2 show the system in OLGA with the PID controller.

Simulation result

Due to time constraints, the PID-controller was only roughly tuned based on trial and error, but it was enough to show that a subsea valve at the riser base works for stabilizing riser slugging in OLGA. In figure 6.3, the topmost simulation show the inlet pressure P_{in} started in an unstable equilibrium point without control, and the pressure starts to oscillate. The other two simulation results show the same experiment done using the PID-controller and the pressure is stabilized.

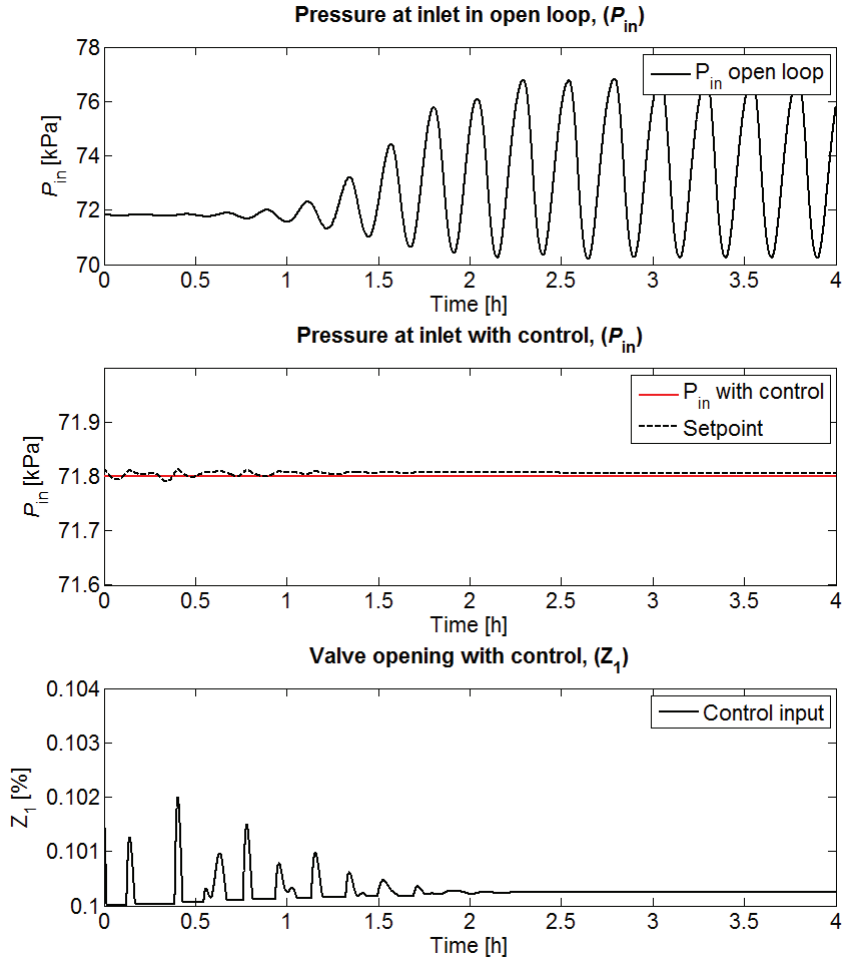

Figure 6.3: OLGA simulation using control using subsea valve compared to open loop

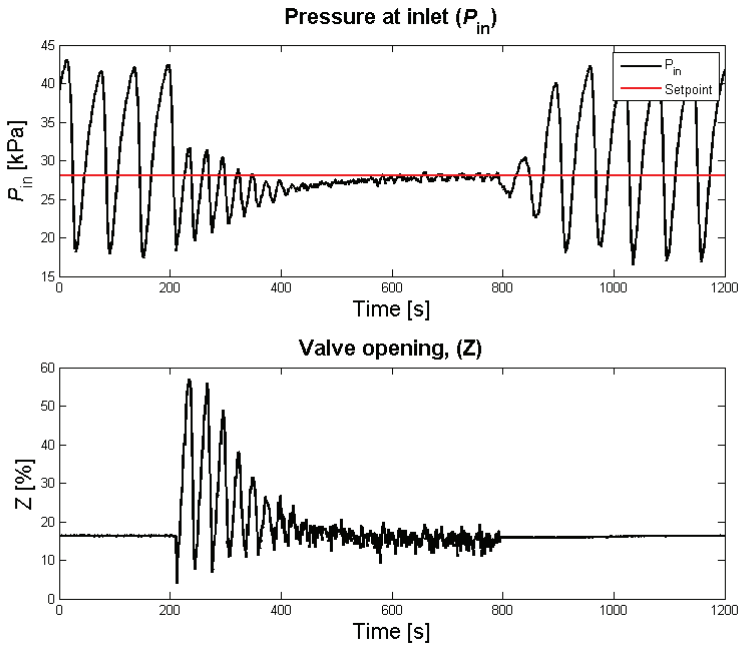

Figure 6.4: Experiment: Slug control using subsea valve on small scale flow lab

6.2 Experimental

A small scale flow lab used for studying riser slugging located at NTNU were used for anti-slug control experiments using a topside choke valve in an earlier project assignment. A description of the lab can be found in the report [9]. This lab has later been modified to include a subsea valve at the riser base, a setup similar to that of figure 6.1.

Figure 6.4 show an experiment done on the flow lab using a subsea valve located at the riser base in a control setup with a PI-controller and the inlet pressure P_{in} as CV. The controller starts in manual mode, and the pressure oscillations indicate riser slugging. After about 200 seconds, the controller is switched to automatic mode and stabilizes the flow in about 400 seconds. After 800 seconds, the controller is switched back to manual and riser slugging is again observed.

7 Discussion

In this thesis, a simplified 5-state model of a well-pipeline riser system have been used for a controllability analysis to find out if the a subsea valve located at the riser base is suitable to control riser slugging. The controllability analysis in part II showed that the subsea valve not had much influence on the different measurement variables proposed as candidate CVs, and the γ-values indicated that the subsea valve would perform worse than the topside valve, which is usually used for riser slugging control.

The simulations in part III showed that the $\mathcal{H}_\infty$-controllers developed were very unrobust when used with the subsea valve, and small disturbances from the operating point they were designed for, would make the system go unstable. The test simulations done in OLGA were unsuccessful in stabilizing the riser slugging, and this is another indication that a subsea valve at the wellhead is unsuitable for controlling riser slugging.

The fact that we were able to keep the flow stable in simulations on the simplified model and not the OLGA-model is perhaps because the simplified model is to simple to describe the dynamics of the long pipeline. The simplified model could possibly be modified to model this better by using several control volumes in the model of the pipeline.

A lot of time were used on testing riser slugging using the subsea valve in OLGA, but when this did not work, very little time was left to test the configuration were the subsea valve was located near the riser base. Therefore, a further investigation of this proposed as further work.

Further work

In chapter 6 we saw that a valve closer to the riser base would be a better location for a subsea valve used for stabilizing riser slugging. To better investigate which controlled variables that could be suitable for this valve, one could change the 5-state simplified model to include a valve in this position, and do a similar controllability analysis as done is this thesis. A small scale flow lab equipped with a subsea valve is available at NTNU, so this could also be used in an experimental study.

In addition, some of the measurements used as candidate CVs in this thesis may be unobtainable in a real offshore plant, so an interesting project could also be to use an estimator to estimate these measurements and test them in an anti-slug controller.

8 Conclusion

This thesis has investigated if a subsea valve located at the wellhead could be used for controlling riser slugging. Based on an input-output controllability analysis on the simplified model of a well-pipeline-riser system presented in chapter 2.2, wee found that when the slugging originates in the riser base, the subsea valve is not as good as the topside valve when used for anti-slug control.

Based on the results from the analysis found in table 4, the simplified model was used for simulations with an anti-slug controller, where the most promising measurements from the analysis were used as controlled variables. The performance of the controller using the subsea valve was unsatisfactory, as it was only able to keep the flow stable for small disturbances around the operating point.

As seen in table 7, several different control structures using the subsea valve was tested in the flow simulator OLGA, both using a single feedback loop and cascade controllers, but neither of them were able to stabilize the slugging. All these results indicates that for anti-slug control of slugging in the riser, the subsea valve is unsuitable.

References

[1] Ove Bratland. *Pipe Flow 2: Multi-phase Flow Assurance*. Ove Bratland, 2010.

[2] J. Chen. Logarithmic integrals, interpolation bounds, and performance limitations in mimo feedback systems. *Automatic Control, IEEE Transactions on*, 45(6):1098–1115, 2000.

[3] Keith Glover. Robust stabilization of linear multivariable systems: relations to approximation. *International Journal of Control*, 43(3):741–766, 1986.

[4] D.W. Gu, P.H. Petkov, and M.M. Konstantinov. *Robust control design with MATLAB*, volume 1. Springer Verlag, 2005.

[5] S. E. Haaland. Simple and explicit formulas for the friction factor in turbulent pipe flow. *Journal of Fluids Engineering*, 105(1):89–90, 1983.

[6] K. Havre, K.O. Stornes, and H. Stray. Taming slug flow in pipelines. *ABB review*, 4:55–63, 2000.

[7] E. Jahanshahi and S. Skogestad. Simplified dynamical models for control of severe slugging in multiphase risers. In *18th IFAC World Congress*, pages 1634–1639, Milan, Italy, Auguest 2011.

[8] E. Jahanshahi, S. Skogestad, and A. H. Helgesen. Controllability analysis of severe slugging in well-pipeline-riser systems. In *IFAC Workshop - Automatic Control in Offshore Oil and Gas Production*, Trondheim, Norway, May 2012.

[9] Mats Lieungh. Experimental study of anti-slug control in pipeline-riser systems, 2011.

[10] MATLAB. *version 7.13.0 (R2011b)*. The MathWorks Inc., Natick, Massachusetts, 2011.

[11] Lieungh Mats. Matlab code: http://www.nt.ntnu.no/users/skoge/diplom/diplom12/, June 2012.

[12] Florent Di Meglio. *Dynamics and control of slugging in oil production*. PhD thesis, Ecole des Mines de Paris, 2011.

[13] G. Skofteland, J-M. Godhavn, and T. Kulset. Implementation of a slug control system for subsea wells in an integrated operation environment. In *10th BHR Conference on Multiphase flow*, Edinburgh, UK., 2007.

[14] S. Skogestad and I. Postletwaite. *Multivariable Feedback Control, Analysis and Design, Second Edition*. John Wiley and Sons, Ltd, 2005.

[15] SPT-Group. *OLGA 5 User Manual*. SPT Group, 2006.

[16] E. Storkaas. *Anti-slug control in pipeline-riser systems*. PhD thesis, PhD thesis, Norwegian University of Science and Technology, 2005.

A Simplified model equations

A.1 Well model

Assuming no inter-phase mass transport in the subsea choke valve, the gas mass fraction at top of the well is equal to the gas mass fraction at inlet of the pipeline given by equation (A.26) in the pipeline model.

$$\alpha^m_{gw,t} = \bar{\alpha}^m_{gp} \tag{A.1}$$

Average gas mass fraction in the well is directly related to gas mass fraction at top of the well.

$$\bar{\alpha}^m_{gw} = K_w \alpha^m_{gw,t}/2, \tag{A.2}$$

where $K_w \approxeq 1$ is a fitting parameter. The mass of individual phases in the well can be calculated as follows.

$$m_{gw} = \bar{\alpha}^m_{gw} m_{tw} \tag{A.3}$$

$$m_{lw} = (1 - \bar{\alpha}^m_{gw}) m_{tw} \tag{A.4}$$

Volume of gas in well:

$$V_{gw} = V_w - \frac{m_{lw}}{\rho_l} \tag{A.5}$$

Wellhead pressure:

$$P_{wh} = \frac{m_{gw} R T_{wh}}{M_G V_w} \tag{A.6}$$

Density of gas phase:

$$\rho_{gw} = \frac{m_{gw}}{V_{gw}} \tag{A.7}$$

Density of two-phase mixture:

$$\rho_{mw} = \frac{m_{gw} + m_{lw}}{V_w} \tag{A.8}$$

Average liquid volume fraction in well:

$$\bar{\alpha}_{lw} = \frac{m_{lw}}{\rho_l V_w} \tag{A.9}$$

Average liquid superficial velocity:

$$\bar{U}_{sl,w} = \frac{\bar{w}_r}{\rho_l A_w} \tag{A.10}$$

Reynolds number in well:

$$Re_w = \frac{\rho_l \bar{U}_{sl,w} D_w}{\mu} \tag{A.11}$$

Friction factor in well ([5]):

$$\frac{1}{\sqrt{\lambda_w}} = -1.8 \log_{10} \left[\left(\frac{\epsilon / D_w}{3.7} \right)^{1.11} + \frac{6.9}{Re_w} \right] \tag{A.12}$$

Pressure loss due to friction in well:

$$F_w = \frac{\lambda_w \rho_l \bar{U}_{sl,w}^2 l_w}{2 D_w} \tag{A.13}$$

Bottom hole pressure of well:

$$P_{bh} = P_{wh} + \rho_{mw} g L_w + F_w \tag{A.14}$$

Mass flow rate from reservoir:

$$w_r = PI \max(P_r - P_{bh}, 0) \tag{A.15}$$

Volume fractions at the top of the well:

$$\alpha_{lw,t} = \frac{(1 - \alpha_{gw,t}^m)\rho_{gw}}{\alpha_{gw,t}^m \rho_l + (1 - \alpha_{gw,t}^m)\rho_{gw}} \tag{A.16}$$

Density of mixture at top of well:

$$\rho_{mw,t} = \alpha_{lw,t} \rho_l + (1 - \alpha_{lw,t}) \rho_{gw} \tag{A.17}$$

A.2 Pipeline inflow conditions

The mass flow rate at the well-head is determined by a subsea choke valve.

$$w_{wh} = K_1 Z_1 \sqrt{\rho_{mw,t} \max(P_{wh} - P_p, 0)}, \tag{A.18}$$

where K_1 is a fitting parameter of the model.
The flow rates of gas and liquid into pipeline are

$$w_{g,in} = w_{wh} \alpha_{gw,t}^m + d_1 \tag{A.19}$$

$$w_{l,in} = w_{wh}(1 - \alpha_{gw,t}^m) + d_2, \tag{A.20}$$

where $d_1$and d_2 are disturbances from the other oil wells to the pipeline.

A.3 Pipeline model

[7] calculated the level of liquid at the low-point from mass of liquid in the pipeline.

$$h_p = \bar{h}_p + \frac{m_{lp} - \rho_l V_p \bar{\alpha}_{lp}}{\pi r_p^2 (1 - \bar{\alpha}_{lp}) \rho_l} \sin(\theta) \tag{A.21}$$

$$\bar{h}_p = K_h \bar{\alpha}_{lp} h_c, \tag{A.22}$$

where $K_h \approxeq 1$ is a fitting parameter.

Volume of gas in pipeline:

$$V_{gp} = V_p - \frac{m_{lp}}{\rho_l} \tag{A.23}$$

Gas density in pipeline:

$$\rho_{gp} = \frac{m_{gp}}{V_{gp}} \tag{A.24}$$

Pressure at inlet of pipeline (ideal gas law):

$$P_p = \frac{\rho_{gp} R T_p}{M_G} \tag{A.25}$$

Average gas mass fraction at inlet of pipeline:

$$\bar{\alpha}_{gp}^m = \frac{(1 - \bar{\alpha}_{lp}) \rho_{gp}}{\bar{\alpha}_{lp} \rho_l + (1 - \bar{\alpha}_{lp}) \rho_{gp}} \tag{A.26}$$

Average liquid superficial velocity:

$$\bar{U}_{sl,p} = \frac{w_{l,in}}{\rho_l A_p} \tag{A.27}$$

Reynolds number in pipeline:

$$Re_p = \frac{\rho_l \bar{U}_{sl,p} D_p}{\mu} \tag{A.28}$$

Friction factor in pipeline ([5]):

$$\frac{1}{\sqrt{\lambda_p}} = -1.8 \log_{10} \left[\left(\frac{\epsilon / D_p}{3.7} \right)^{1.11} + \frac{6.9}{Re_p} \right] \tag{A.29}$$

Pressure loss due to friction in pipeline:

$$F_p = \frac{\lambda_p \rho_l \bar{U}_{sl,p}^2 L_w}{2 D_p} \tag{A.30}$$

A.4 Riser model

Volume of riser:

$$V_r = A_r(L_r + L_h) \tag{A.31}$$

Volume of gas in riser:

$$V_{gr} = V_r - \frac{m_{Lr}}{\rho_L} \tag{A.32}$$

Gas density at top of the riser:

$$\rho_{gr} = \frac{m_{gr}}{V_{gr}} \tag{A.33}$$

Pressure at the top of the riser (ideal gas law):

$$P_{r,t} = \frac{\rho_{gr} R T_r}{M_G} \tag{A.34}$$

Average liquid volume fraction in riser:

$$\bar{\alpha}_{lr} = \frac{m_{lr}}{V_r \rho_l} \tag{A.35}$$

Average density of mixture inside riser:

$$\bar{\rho}_{mr} = \frac{m_{gr} + m_{lr}}{V_r} \tag{A.36}$$

Average mixture velocity in riser:

$$\bar{U}_{mr} = \bar{U}_{sl,r} + \bar{U}_{sg,r} \tag{A.37}$$

$$\bar{U}_{sl,r} = \frac{w_{l,in}}{\rho_l A_r} \tag{A.38}$$

$$\bar{U}_{sg,r} = \frac{w_{g,in}}{\rho_g A_r} \tag{A.39}$$

Reynolds number in riser:

$$Re_r = \frac{\bar{\rho}_m \bar{U}_{mr} D_r}{\mu} \tag{A.40}$$

Friction factor in riser ([5]):

$$\frac{1}{\sqrt{\lambda_r}} = -1.8 \log_{10} \left[\left(\frac{\epsilon / D_r}{3.7} \right)^{1.11} + \frac{6.9}{Re_r} \right] \tag{A.41}$$

Friction loss due to friction in riser:

$$F_r = \frac{\bar{\alpha}_{Lr} \lambda_r \bar{\rho}_{mr} \bar{U}_{mr}^2 (L_r + L_h)}{2 D_r} \tag{A.42}$$

Pressure at bottom of riser:

$$P_{r,b} = P_{r,t} + \rho_{mr} g L_r + F_r \tag{A.43}$$

A.5 Gas flow at low-point

Free area for gas flow through low-point:

$$A_g \approxeq A_p \left(\frac{h_c - h_p}{h_c} \right)^2, \quad h_p < h_c \tag{A.44}$$

Flow rate of gas through low-point:

$$w_{gr,b} = 0, \quad h_p > h_c \tag{A.45a}$$

$$w_{gr,b} = K_g A_g \sqrt{\rho_{gp} \max(0, P_p - P_{r,b})}, \quad h_p < h_c \tag{A.45b}$$

A.6 Liquid flow at low-point

Area of liquid flow through low point:

$$A_l = A_p - A_g \tag{A.46}$$

Liquid flow rate through low-point:

$$w_{lr,b} = K_l A_l \sqrt{\rho_l \max(0, P_p + \rho_l g h_p - P_{r,b})} \tag{A.47}$$

A.7 Outflow conditions

Liquid volume fraction at top of riser ([7]):

$$\alpha_{lr,t} = 2\bar{\alpha}_{lr} - \frac{A_l}{A_p} \tag{A.48}$$

Density of mixture at the top of riser:

$$\rho_{mr,t} = \alpha_{lr,t}\rho_l + (1 - \alpha_{lr,t})\rho_{gr} \tag{A.49}$$

Gas mass fraction at top of riser:

$$\alpha^m_{gr,t} = \frac{(1 - \alpha_{lr,t})\rho_{gr}}{\alpha_{lr,t}\rho_l + (1 - \alpha_{lr,t})\rho_{gr}} \tag{A.50}$$

Flow rate of outlet mixture:

$$w_{out} = K_{pc} Z_2 \sqrt{\rho_{mr,t}(P_{r,t} - P_s)} \tag{A.51}$$

Flow rate of outlet liquid:

$$w_{l,out} = (1 - \alpha^m_{gr,t}) w_{out} \tag{A.52}$$

Flow rate of outlet gas:

$$w_{g,out} = \alpha^m_{gr,t} w_{out} \tag{A.53}$$

The constants and parameter values of the model are given in Table 8.

Table 8: Constants and parameters values

Symb.	Description	Values	Units
R	universal gas constant	8314	$J/(kmol.K)$
g	gravity	9.81	m/s^2
μ	viscosity	1.426×10^{-4}	$Pa.s$
ρ_l	liquid density	832.2	kg/m^3
θ	pipe inclination	1	deg
D_w	well diameter	0.12	m
D_p	pipeline diameter	0.12	m
D_r	riser diameter	0.1	m
h_c	critical liquid level	$D_p/cos(\theta)$	m
A_w	well cross section area	0.0113	m^2
A_p	pipe cross section area	0.0113	m^2
A_r	riser cross section area	0.0079	m^2
L_w	depth of oil well	3000	m
L_p	pipeline length	4300	m
L_r	pipeline length	4300	m
L_h	horizontal section length	100	m
T_w	well temperature	369	K
T_p	pipeline temperature	337	K
T_p	pipeline temperature	337	K
T_r	riser temperature	298.3	K
M_G	gas molecular weight	20	gr
P_r	reservoir pressure	320	bara
P_s	separator pressure	50.1	bara
PI	productivity index	2.75×10^{-6}	$kg/(s.Pa)$
V_w	volume of oil well	33.93	m^3
V_p	volume of pipeline	48.64	m^3
V_r	volume of riser	3.14	m^3
K_1	subsea choke cons.	0.014	–
K_2	top-side choke cons.	0.011	–
K_h	low point tuning parameter	0.6	–
K_g	low point tuning parameter	0.030	–
K_o	low point tuning parameter	0.236	–
K_a	well tuning parameter	0.904	–

B Bifurcation diagrams

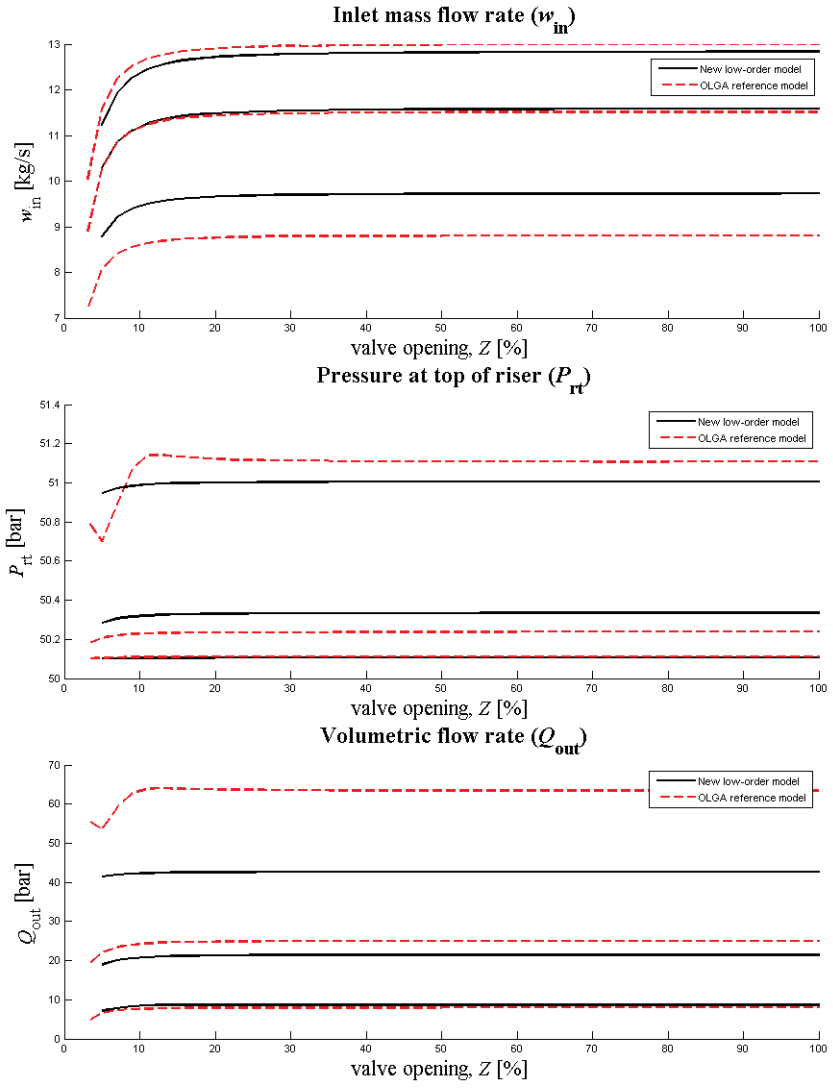

Figure B.1: Bifurcation diagrams with the subsea valve z_1 as bifurcation parameter. The topside valve were kept constant at $z_1 = 30\%$.

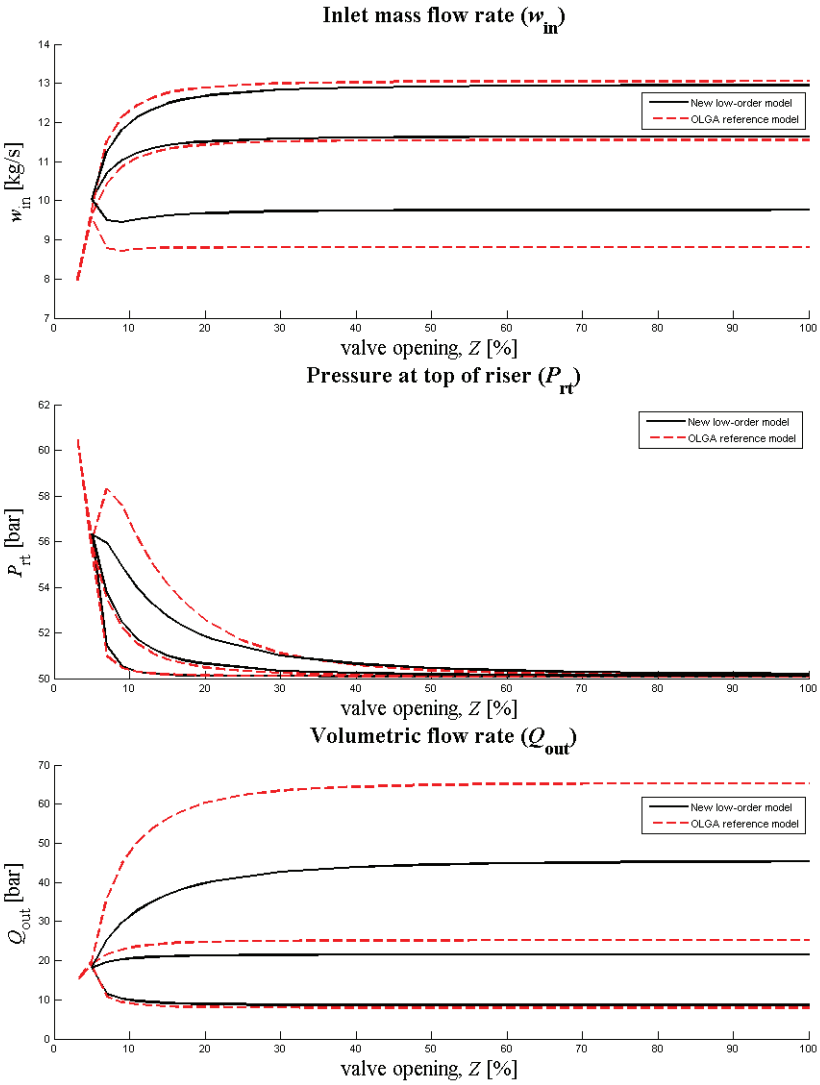

Figure B.2: Bifurcation diagrams with the topside valve z_2 as bifurcation parameter. The subsea valve were kept constant at $z_1 = 100\%$.

C Matlab Examples

Controllability

```
%% **** System Inputs ****
par = v2_new_5d_parameters(); %All parameters defined in one file
z1 = 0.1; % Subsea valve
z2 = 0.1; % Topside valve
global u0;
u0 = [z1;z2;0;0];
%% ******** Initialization *************
[x0,y0,par] =  v2_new_5d_initialize(u0,par); % Find steady state values
%% ******** Linearization *************
[A,B,C,D]=v2_new_5d_linmodl_num(x0,u0,par); % Numerical linearization
                                            %around operating point
sys =ss(A,B,C,D);
set(sys,'inputname',{'Z1','Z2','d1','d2'},'outputname',{'P_bh','P_wh',...
    'W_in','P_in','P_rb','DP_r','P_t','Q_out','W_out','Rho_t','Alpha_L'},...
    'statename',{'m_Gw','m_Gp','m_Lp','m_Gr','m_Lr'});
%% ****Scaling****
[De,Dd,Du] = scaling(z1,z2);

Bs1 = B(:,1:2)*Du;
Bs2 = B(:,3:4)*Dd;
Bs = [Bs1 Bs2];

Cs = (De^-1)*C;

Ds1 = (De^-1)*D(:,1:2)*Du;
Ds2 = (De^-1)*D(:,3:4)*Dd;
Ds = [Ds1 Ds2];
%% Define system names
sys =(ss(A,Bs,Cs,Ds));
set(sys,'inputname',{'Z1','Z2','d1','d2'},'outputname',{'P_bh','P_wh',...
    'W_in','P_in','P_rb','DP_r','P_t','Q_out','W_out','Rho_t','Alpha_L'},...
    'statename',{'m_Gw','m_Gp','m_Lp','m_Gr','m_Lr'});
sys = minreal(sys);
Gu = tf(sys({'P_bh','P_wh','W_in','P_in','P_rb','DP_r','P_t','Q_out',...
    'W_out','Rho_t','Alpha_L'},'Z1'));
```

```
Gd = tf(sys({'P_bh','P_wh','W_in','P_in','P_rb','DP_r','P_t','Q_out',...
    'W_out','Rho_t','Alpha_L'},{'d1','d2'}));

%% Sensitivity peak for P_bh.
sys1 = sys('P_bh','Z1');
[p, z1]=pzmap(sys1);
RHPp1=p(find(p>0));
RHPz1=z1(find(z1>0));
l=1;
if (isempty(RHPp1) || isempty(RHPz1))
    Msmin1=1;
else
    np1=length(RHPp1); nz1=length(RHPz1);
    [V,E]=eig(A); V=V(:,find(diag(E)>0));
    Yp1 = zeros(l,np1);
    Yz1 = zeros(l,nz1);
    for i=1:np1
        Yp1(:,i) = Cs(1,:)*V(:,i)/norm(Cs(1,:)*V(:,i));%Pole direction
    end
    for j=1:nz1
        [U,S,V]=svd(evalfr(G1,RHPz1(j))); Yz1(:,j)=U(:,end);%Zero direction
    end
    Qz1 = zeros(nz1,nz1); Qp1 = zeros(np1,np1); Qzp1 = zeros(nz1,np1);
    for i=1:nz1
        for j=1:nz1
            Qz1(i,j) = ctranspose(Yz1(:,i))*Yz1(:,j)/...
                (RHPz1(i)+conj(RHPz1(j)));
        end
    end
    for i=1:np1
        for j=1:np1
            Qp1(i,j) = ctranspose(Yp1(:,i))*Yp1(:,j)/...
                (conj(RHPp1(i))+RHPp1(j));
        end
    end
    for i=1:nz1
        for j=1:np1
            Qzp1(i,j) = ctranspose(Yz1(:,i))*Yp1(:,j)/...
                (RHPz1(i)-RHPp1(j));
```

```
        end
    end

    Msmin1=sqrt(1+norm(sqrtm(inv(Qz1))*Qzp1*sqrtm(inv(Qp1)))^2);
end
```

$\mathcal{H}_\infty$-controller and $\gamma - value$

```
%% H-infinity optimal controller for plant
% Transfer functions from Z1 valve
Gc = tf(sysc({'P_bh','P_wh','W_in','P_in','P_rb','DP_r','P_t','Q_out',...
    'W_out','Rho_t','Alpha_L'},'Z1'));

NMEAS = 1; % Number of measurements used
NCON = 1; % Number of control inpus used

% Find H-infinity optimal controller

% Weighting matrix Wp
W1 = [Wp2 zeros(1,10) % Integral action on P_bh
      0 Wp1 zeros(1,9)
      zeros(1,2) Wp1 zeros(1,8)
      zeros(1,3) Wp1 zeros(1,7)
      zeros(1,4) Wp1 zeros(1,6)
      zeros(1,5) Wp1 zeros(1,5)
      zeros(1,6) Wp1 zeros(1,4)
      zeros(1,7) Wp1 zeros(1,3)
      zeros(1,8) Wp1 zeros(1,2)
      zeros(1,9) Wp1 0
      zeros(1,10) Wp1];

% Weighting matrix Wu
W2 = repmat(Wu,11,1);

% Weighting matrix Wt
W3 = [Wt zeros(1,10)
      0 Wt zeros(1,9)
      zeros(1,2) Wt zeros(1,8)
      zeros(1,3) Wt zeros(1,7)
```

```
      zeros(1,4) Wt zeros(1,6)
      zeros(1,5) Wt zeros(1,5)
      zeros(1,6) Wt zeros(1,4)
      zeros(1,7) Wt zeros(1,3)
      zeros(1,8) Wt zeros(1,2)
      zeros(1,9) Wt 0
      zeros(1,10) Wt];

% Generalized Plant P
P = augw(Gc,W1,W2,W3);
P = minreal(P(1:34,:));

%Calculate H_inf controller and display gamma-value
[K,CL,GAM,INFO] = hinfsyn(P,NMEAS,NCON,'TOLGAM',1e-6,'METHOD','ric',...
    'DISPLAY','on');
disp(GAM);
```

D Controllability analysis - Tables

The controllability results done is this thesis were also done around a second operating point, $Z_1 = 30\%$ and $Z_2 = 10\%$.

Measurement	Value	D_y	$G(0)$	$\lvert S\rvert = \lvert T\rvert$	$\lvert KS\rvert$	$\lvert SG\rvert$	$\lvert KSG_{d1}\rvert$	$\lvert KSG_{d2}\rvert$	$\lvert SG_{d1}\rvert$	$\lvert SG_{d2}\rvert$	γ
P_{bh}	279.62	1	-0.286	2.82	8.39	0.73	1.49	3.28	0.24	0.52	218
P_{wh}	71.25	1	-0.173	2.15	8.79	0.32	1.49	3.28	0.18	0.39	227
W_{in}	11.11	1	0.079	5.62	27.42	1.02	1.49	3.28	0.21	0.47	755
P_{in}	71.13	1	0.058	1	8.74	0	1.49	3.28	0	0	223
P_{rb}	68.79	1	0.025	1.37	7.33	0.41	1.43	3.88	0.04	0.26	197
DP_r	16.76	1	-0.002	1.02	5.50	0.18	1.12	3.31	0.28	0.23	171
P_t	52.03	1	0.028	1.71	12.04	0.10	1.11	3.86	0.09	0.24	429
Q_{out}	20.47	2	0.073	1.65	4.80	1.33	1.49	3.78	0.26	0.52	165
W_{out}	11.11	1	0.079	1.76	3.66	0.35	1.11	4.03	0.22	0.87	129
ρ_t	542.43	50	-0.001	2.04	6.75	0.24	1.57	4.67	0.23	0.65	193
$\alpha_{L,t}$	0.63	1	0.000	2.05	105.93	0.02	1.57	4.67	0.01	0.04	-
$P_{bh}P_{wh}$				1	6.07	0	0.75	1.64	0	0	158
$P_{bh}W_{in}$				1	8.03	0	0.75	1.64	0	0	210
$P_{bh}P_{in}$				1	6.05	0	0.75	1.64	0	0	158
$P_{wh}W_{in}$				1	8.37	0	0.75	1.64	0	0	217
$P_{wh}P_{in}$				1	6.20	0	0.75	1.64	0	0	160
$W_{in}P_{in}$				1	8.32	0	0.75	1.64	0	0	214

Table 9: Z1 ($Z_1 = 30$, $Z_2 = 10$)

Measurement	Value	D_y	$G(0)$	$\lvert S\rvert = \lvert T\rvert$	$\lvert KS\rvert$	$\lvert SG\rvert$	$\lvert KSG_{d1}\rvert$	$\lvert KSG_{d2}\rvert$	$\lvert SG_{d1}\rvert$	$\lvert SG_{d2}\rvert$	γ
P_{bh}	279.62	1	-3.31	1	0.36	0	0.063	0.139	0	0	20
P_{wh}	71.25	1	-3.16	1	0.37	0	0.063	0.139	0	0	17
W_{in}	11.11	1	0.91	1	1.17	0	0.063	0.139	0	0	45
P_{in}	71.13	1	-3.17	1	0.37	0	0.063	0.139	0	0	17
P_{rb}	68.79	1	-3.55	1	0.31	0	0.061	0.165	0	0	14
DP_r	16.76	1	-0.03	1	0.23	0	0.048	0.140	0	0	100
P_t	52.03	1	-3.52	2.30	0.51	4.47	0.047	0.164	0.083	0.309	33
Q_{out}	20.47	2	0.94	1	0.20	0	0.063	0.161	0	0	34
W_{out}	11.11	1	0.91	1	0.16	0	0.047	0.171	0	0	35
ρ_t	542.43	50	-0.11	2.04	0.29	5.68	0.067	0.198	0.232	0.661	95
$\alpha_{L,t}$	0.63	1	-0.01	2.04	4.50	0.36	0.067	0.198	0.015	0.042	201
$P_{in}P_t$				1	0.30	0	0.030	0.077	0	0	13
$P_{in}W_{out}$				1	0.14	0	0.030	0.080	0	0	11
P_tW_{out}				1	0.14	0	0.030	0.080	0	0	14
$P_t\rho_m$				1	0.15	0	0.024	0.084	0	0	18
$P_{bh}W_{out}$				1	0.25	0	0.034	0.099	0	0	10

Table 10: Z2 ($Z_1 = 30$, $Z_2 = 10$)

Measurement	$\|S\| = \|T\|$	$\|KS\|$	$\|SG\|$	$\|KSG_{d1}\|$	$\|KSG_{d2}\|$	$\|SG_{d1}\|$	$\|SG_{d2}\|$	γ_1	γ_2	γ_3
$P_{bh}P_{in}$	1	0.22	0	0.024	0.054	0	0	9	9	80
$P_{bh}P_{rb}$	1.01	0.20	0.01	0.025	0.056	0.003	0.004	8	8	82
$P_{bh}P_t$	1.28	0.23	2.80	0.028	0.064	0.177	0.499	9	14	81
$P_{bh}W_{out}$	1.09	0.13	0.01	0.028	0.068	0.039	0.268	6	14	100
$P_{wh}P_{rb}$	1.02	0.20	0.05	0.025	0.056	0.009	0.039	8	8	91
$P_{wh}P_t$	1.28	0.24	2.58	0.028	0.064	0.188	0.500	9	15	91
$P_{wh}W_{out}$	1.30	0.13	0.05	0.028	0.068	0.053	0.417	6	14	100
$P_{in}P_t$	1	0.24	0	0.028	0.064	0	0	9	15	100

Table 11: MIMO ($Z_1 = 30$, $Z_2 = 10$)

E Simulation results

E.1 Linear model

Stabilizing control of the linear system using P_{bh} as CV. 5 % disturbance. See figure E.1

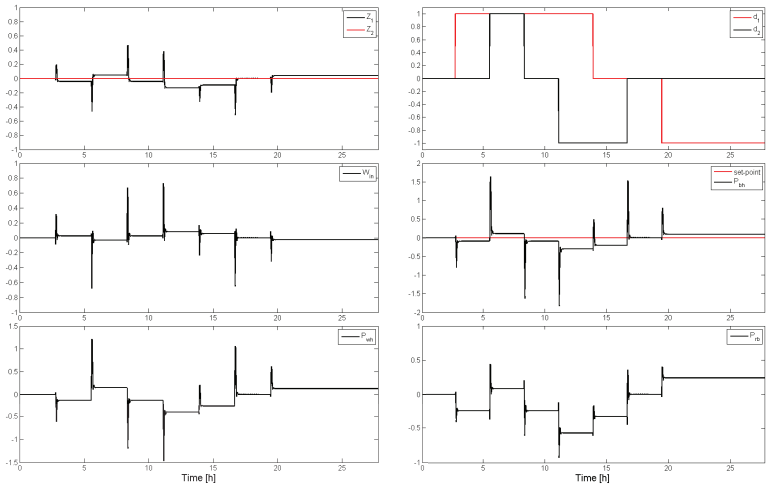

Figure E.1: Control of linear model using P_{bh} as CV

Stabilizing control of the linear system using P_{wh} as CV. 5 % disturbance. See figure E.2

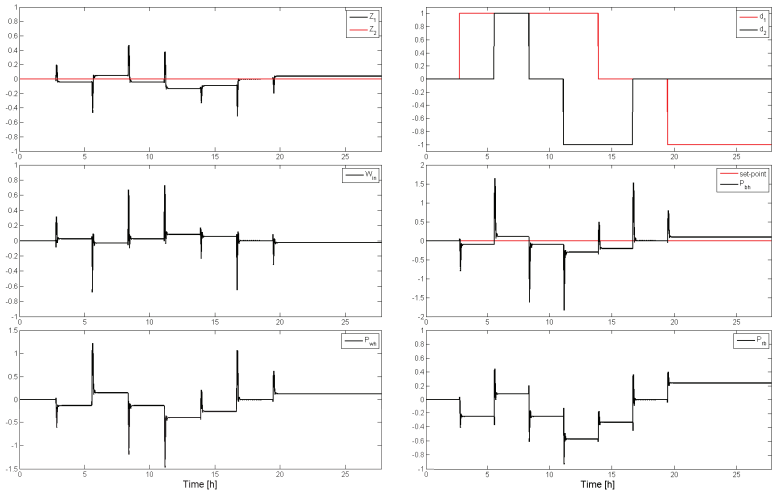

Figure E.2: Control of linear model using P_{wh} as CV

Stabilizing control of the linear system using P_{rb} as CV. 5 % disturbance. See figure E.3.

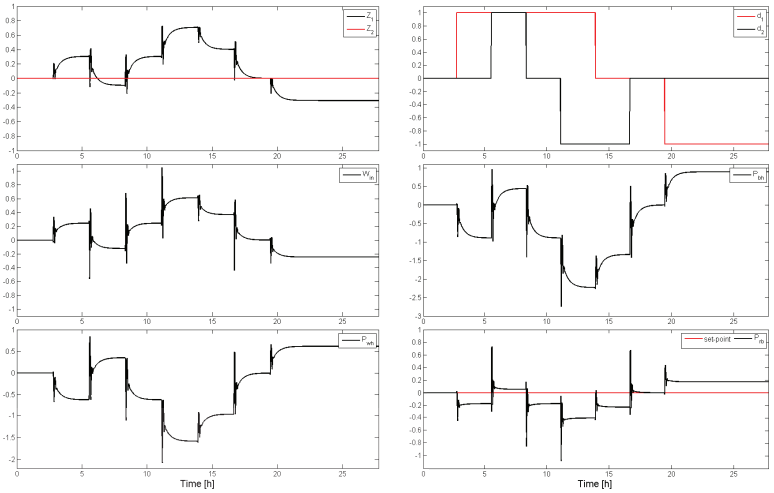

Figure E.3: Control of linear model using P_{rb} as CV

E.2 Nonlinear model

SISO Stabilizing control of the linear system using P_{rb} as CV. 1 % disturbance, see figure E.4.

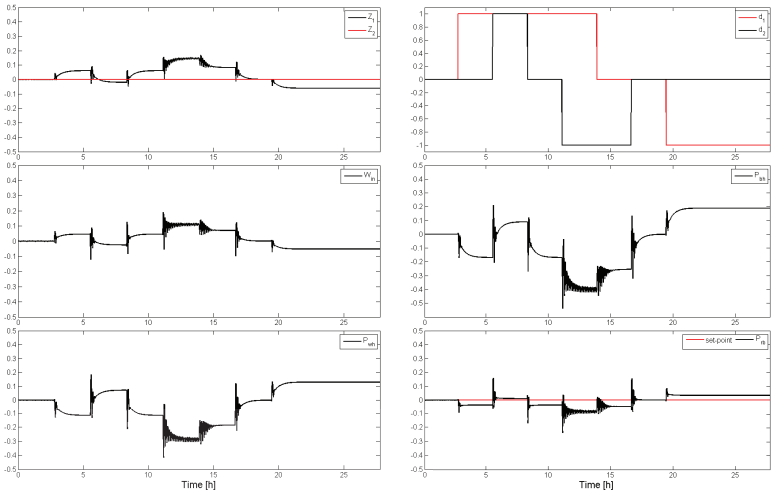

Figure E.4: Control of linear model using P_{rb} as CV

MISO Stabilizing control of the nonlinear system using a combination of P_{bh} and W_{in} as CVs. 1 % disturbance. See figure E.5.

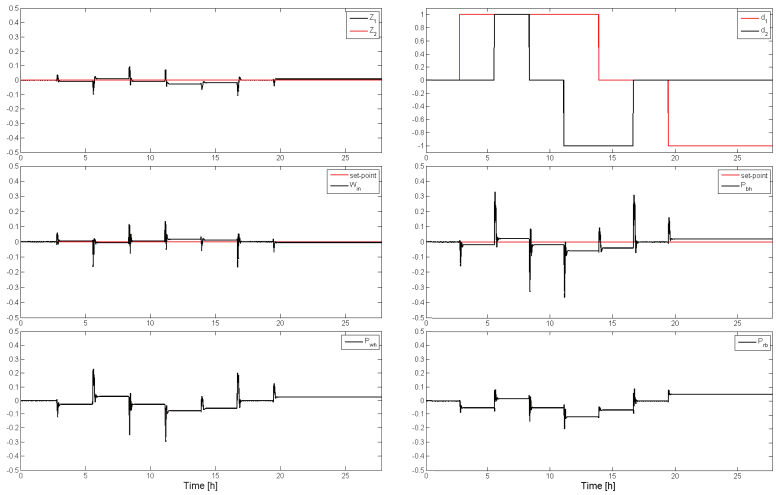

Figure E.5: Control of nonlinear model using P_{bh} and W_{in} as CVs

Stabilizing control of the nonlinear system using a combination of P_{wh} and W_{in} as CVs. 1 % disturbance. See figure E.6.

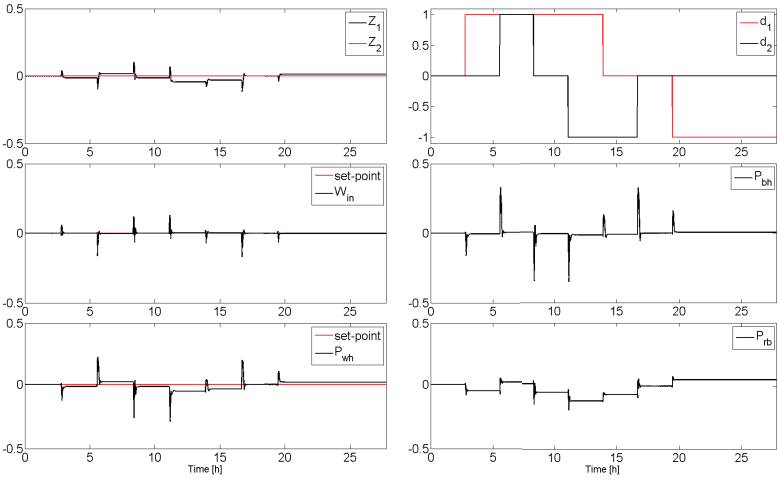

Figure E.6: Control of nonlinear model using P_{wh} and W_{in} as CVs

MIMO Stabilizing control of the nonlinear system using both the subsea and the topside valve using a combination of P_{in} and P_t as CVs. 5 % disturbance. See figure E.7.

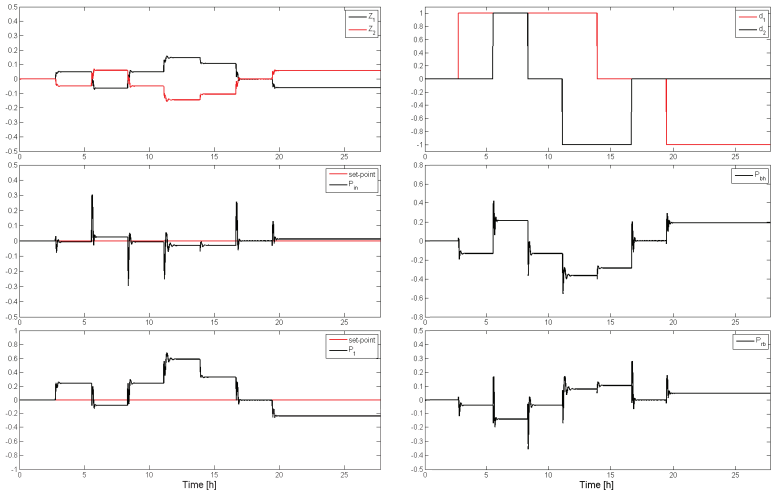

Figure E.7: Control of nonlinear model using both valves and P_{in} and P_t as CVs

Stabilizing control of the nonlinear system using both the subsea and the topside valve using a combination of P_{wh} and P_{rb} as CVs. 5 % disturbance. See figure E.8.

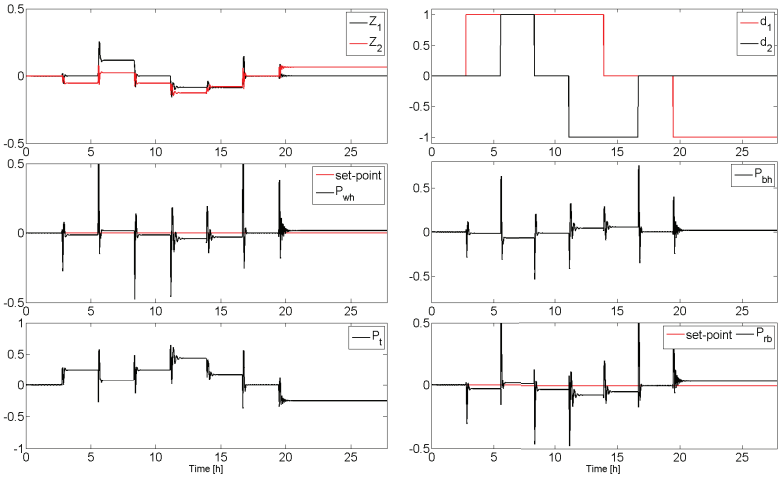

Figure E.8: Control of nonlinear model using both valves and P_{wh} and P_{rb} as CVs